days or 1 or 2 weeks after MI, 3 to 6 mice from each group were killed for analysis. The experiments were performed in accordance with the guidelines established by Chiba University for experiments in animals.

Injection of Plasmids Carrying LIF cDNA

The LIF expression vector was constructed by inserting a chimera of human and mouse LIF cDNA into the pCAGGS plasmid, which is driven by both a cytomegalovirus enhancer and a chicken β-actin promoter.[22] The plasmid was prepared by use of the Concert High Purity Plasmid Purification Systems (Gibco BRL) and injected at a dose of 100 μg plasmids per 100 μL PBS per 20 g body wt into the thigh muscle of mice immediately after MI. The same volume of PBS alone was injected in littermate mice as controls.

Assay of LIF Concentration

Plasma LIF concentration was measured with a ELISA kit (Quantikine M) according to the manufacturer's instructions. The LIF ELISA kit has high sensitivity by which the minimum 2 pg/mL of LIF can be detectable. The assay of this kit is specific for natural and recombinant mouse LIF.

Echocardiography

Transthoracic echocardiography was performed with an Agilent Sonos 4500 (Agilent Technologies Co) provided with an 11-MHz imaging transducer. When the mice had partially recovered from the light anesthesia, M-mode images of the left ventricle (LV) were recorded.[21]

Histology

Hearts fixed in 10% formalin were embedded in paraffin, sectioned at 4-μm thickness, and stained with hematoxylin-eosin and Azan. The extent of fibrosis was measured in 10 fields randomly selected from the LV free wall (LVFW) of each section. Five sections from each heart were measured, and the value was expressed as the ratio of Azan-stained fibrosis area to total myocardium area. The "remained myocardium" in the ischemic area was determined from 5 sections for each heart by calculating the ratio of (LVFW area−fibrotic area) divided by LVFW area.

TUNEL Analysis

Cardiomyocyte death was assessed in situ by terminal deoxyribonucleotide transferase (TdT)-mediated dUTP nick end-labeling (TUNEL) of paraffin-embedded heart sections using Cardio TACS (Trevigen Inc).

Isolation and Transplantation of BMCs

BMCs were isolated from 8-week-old male transgenic mice (C57BL/6) systemically overexpressing green fluorescent protein (GFP), a kind gift from M. Okabe.[23,24] BMCs (5×10^7) suspended in 300 μL of RPMI medium were injected intravenously into each 8-week-old female C57BL/6 mouse whose total body had been irradiated (9 Gy) for 6 hours. Six weeks after BMC transplantation, the mice were operated on to induce MI. A flow cytometric analysis using an EPICS ALTRA (Beckman Coulter) equipped with a 525-nm filter at a bandwidth of ±15 nm revealed that >70% of BMCs were derived from donor cells.

Immunohistochemistry and Western Blotting

Paraffin-embedded cardiac sections were immunohistochemically stained by use of antibodies to Ki-67 (Dako), GFP (MBL, Japan), platelet and endothelial cell adhesion molecule (PECAM)-1, and cardiac troponin T (cTnT) (Santa Cruz) and MF20, and then with secondary antibodies conjugated with biotin, FITC, or rhodamine. Western blot analysis was performed with antibodies to vascular endothelial growth factor (VEGF) (Santa Cruz). Hybridizing bands were visualized by use of an enzyme-linked chemiluminescence detecting kit (Amersham Pharmacia Biotech).

Fluorescence In Situ Hybridization for Y Chromosome

Fluorescence in situ hybridization (FISH) for the Y chromosome was performed by use of the Y chromosome probe pUC18-Y351B, a kind gift from C.E. Bishop (Department of Obstetrics and Gynecology, Baylor College of Medicine, Houston, Tex).[25] Engraftment of cardiomyocytes was assessed by FISH on paraffin-embedded cardiac sections after immunostaining for cTnT. Cardiac sections from normal male and female mice served as positive and negative controls, respectively.

Statistical Analysis

All values are expressed as mean±SD of 3 experiments in each instance. Comparisons were made by 1-way ANOVA followed by the Dunnett modified t test. Differences with a value of $P<0.05$ were considered statistically significant.

Results

Increases in LIF Proteins After Injection of LIF cDNA

Some cytokines, including the IL-6 family, have been reported to be increased in MI.[26,27] We first examined LIF protein concentrations in blood of mice after inducing MI. Endogenous plasma LIF concentrations were increased transiently after MI (before, 0.06 ng/mL; 2 days, 2.1 ng/mL; 1 week, 0.8 ng/mL; 2 weeks, 0.4 ng/mL; 4 weeks, 0.13 ng/mL). In mice that were injected with LIF plasmid DNA into the thigh muscle immediately after MI had been induced, LIF protein was markedly increased. The concentrations of LIF peaked at 1 week (5.3 ng/mL) after the injection of LIF cDNA and remained persistently high for >4 weeks (1.4 ng/mL).

Attenuation of Infarct Extent and LV Remodeling and Improvement of Cardiac Function by LIF

To elucidate whether an increase in LIF protein has beneficial effects on MI, we assessed cardiac function and morphology by echocardiography at 2 weeks after MI. In vehicle-injected MI mice, the posterior wall thickness of the LV was decreased significantly compared with sham-operated mice, and the thickness of the interventricular septum was conversely increased (Table). Moreover, LV internal dimensions at both end-diastole and end-systole were increased, whereas the fractional shortening and ejection fraction were decreased (Table), suggesting that LV remodeling and cardiac dysfunction occurred after MI. In LIF cDNA–injected MI mice, all these changes were less prominent and cardiac functions were much better than in vehicle-injected mice (Table). In vehicle-injected MI mice, the infarction area was quite large and the LVFW was very thin (Figure 1A). Fibrosis was so prominent that there were only a few cardiomyocytes in the infarct zone (Figure 1, A and B). In contrast, in LIF cDNA–injected mice, the cardiac muscle was preserved and the LVFW was much thicker (Figure 1A). Fibrosis was less remarkable in the ischemic zone (Figure 1, A and B). All these findings suggest that LIF does exert beneficial effects on MI from the viewpoints of cardiac morphology and function.

Protection Against Cardiomyocyte Death and Induction of Neovascularization by LIF

Because LIF has been reported to protect cardiomyocytes from injury,[16,18] we examined, by use of the TUNEL method,

M-Mode Echocardiographic Analysis After 2 Weeks of MI

	PBS		LIF	
	Sham	MI	Sham	MI
n	3	6	3	7
BW, g	25.0±1.3	23.4±1.0	24.2±0.5	22.0±1.2
HW/BW, mg/g	5.0±0.5	7.5±1.3*	5.2±0.5	6.6±0.6*
IVSTd, mm	0.50±0.02	0.81±0.13*	0.52±0.03	0.76±0.15*†
LVPWTd, mm	0.57±0.01	0.33±0.13*	0.60±0.02	0.45±0.17*†
LVIDd, mm	3.21±0.37	4.87±0.63*	3.12±0.35	3.83±0.38*†
LVIDs, mm	1.74±0.35	3.47±0.4*	1.67±0.34	2.96±0.34*†
EF, %	87±7.0	54±8.0*	89±7.0	70±6.0*†
FS, %	60±1.8	32±4.8*	60±2.0	51±2.3*†

BW indicates body weight; HW, heart weight; IVSTd, interventricular septum thickness; LVPWTd, LV posterior wall thickness; LVIDd and LVIDs, LV internal dimensions at end diastole and end systole, respectively; EF, ejection fraction; and FS, fractional shortening. Data are expressed as mean±SD.
*$P<0.05$ vs sham-operated mice.
†$P<0.05$ vs MI with PBS injection.

whether LIF prevents cardiomyocytes from death at MI. Many TUNEL-positive cardiomyocytes were observed in the border zone of the infarcted heart (Figure 2A). The number of TUNEL-labeled cardiomyocytes was significantly less in LIF-treated mice than saline-injected mice (Figure 2, A and B), indicating that LIF protects cardiomyocytes from death after MI.

Myocardial ischemia is a major cause of cardiomyocyte death. Activation of gp130 signaling has been reported to promote neovascularization in the myocardium.[28] We therefore examined whether LIF induced new vessel formation in the heart after MI. We used PECAM-1 as a marker for neovascularization.[29,30] Immunohistochemical analysis using anti-PECAM antibody revealed that there was more newly

formed vasculature in the border zone of LIF-treated mice than in vehicle-treated mice (Figure 3, A and B). Because VEGF is the most potent angiogenic factor,[31] we examined the expression of VEGF protein in the myocardium after MI. At 1 week after MI, VEGF was slightly upregulated in the hearts of vehicle-treated mice, whereas a marked increase in VEGF was observed in the heart of LIF-injected mice (Figure 3C). These findings suggest that LIF enhanced neovascular-
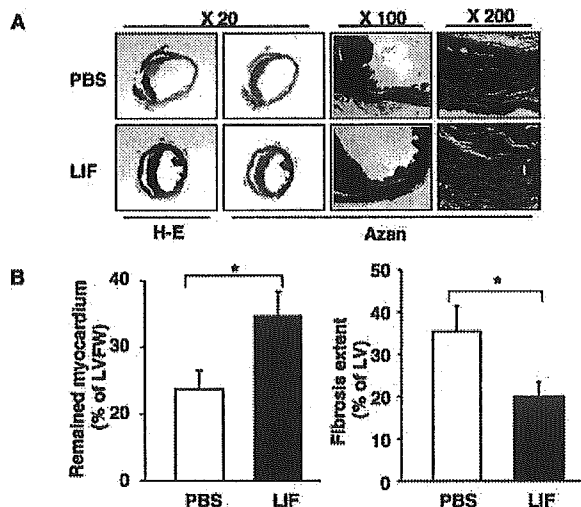
Figure 1. Left ventricular remodeling after 2 weeks of MI. A, Cardiac morphology. Fixed hearts were stained with hematoxylin-eosin (H-E) and Azan. Representative photographs are shown. B, Size of remained myocardium and extent of fibrosis were measured as described in Methods. Data are shown as mean ± SD of 3 hearts. *$P<0.05$.
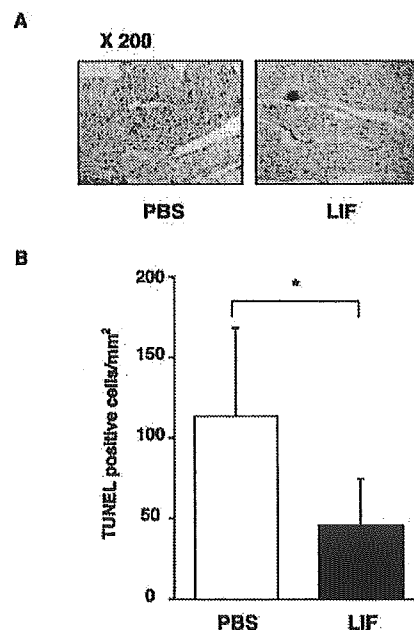
Figure 2. TUNEL analysis after 2 weeks of MI. A, Representative TUNEL staining of heart. Brown staining indicates TUNEL-positive nuclei. B, Number of TUNEL-positive cardiomyocytes counted in 20 fields randomly selected from LVFW of each section. Ten sections from each heart were measured; values are expressed as number of dead cells per mm² of LVFW area. Data are shown as mean ± SD of 3 hearts. *$P<0.05$.
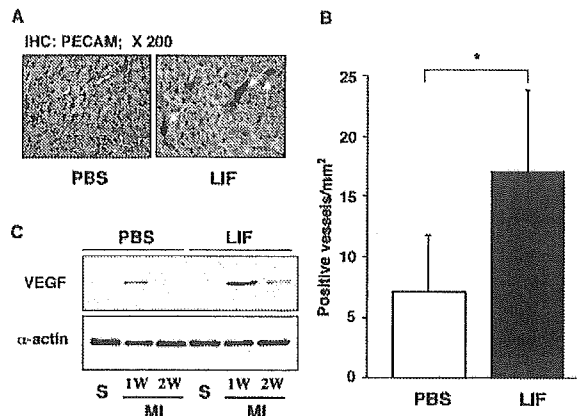
A

IHC: PECAM; X 200

PBS   LIF

C   PBS   LIF

VEGF

α-actin

S $\frac{1W\ 2W}{MI}$ S $\frac{1W\ 2W}{MI}$

B

Figure 3. Neovascularization after 2 weeks of MI. A, Representative photographs showing immunohistochemical (IHC) staining with anti-PECAM antibody in hearts. Arrows indicate PECAM-positive vessels. B, Number of PECAM-positive vessels counted in 20 randomly selected fields from LVFW for each section. Ten sections per heart were counted; values are expressed as number of PECAM-positive vessels per mm^2 of LVFW. Data are shown as mean ± SD of 3 mice. *$P<0.05$. C, Expression of VEGF. Total proteins extracted from LV tissue excised at indicated time points after MI were separated in 12% SDS gels, and blotted membranes were incubated with anti-VEGF antibody or anti-α-actin antibody as an internal control. Representative autoradiograms from 3 independent experiments are shown.

Figure 4. Number of Ki-67–positive cardiomyocytes in cell cycle after 1 week of MI. Ki-67–positive cardiac nuclei were counted in 20 fields randomly selected from LVFW for each section. Twenty sections from each heart were measured. Values are expressed as number per mm^2 of LVFW area. Data are shown as mean ± SD of 3 mice. *$P<0.05$.

ization in the infarcted myocardium, at least in part through the upregulation of VEGF expression.

Proliferation of Cardiomyocytes and Differentiation of BMCs Into Cardiomyocytes

The IL-6 family of cytokines has been reported to promote growth and proliferation of many types of cells, including cardiomyocytes.[9,15,17,19,20] We next examined whether LIF stimulated the proliferation of cardiomyocytes after MI. To identify the cardiomyocytes that had entered the cell cycle, we examined the expression of Ki-67 protein, which has been reported to be expressed only in the nucleus of proliferating cells.[32,33] Only a small number of Ki-67–positive cardiomyocytes were recognized in the border zone of vehicle-treated mice (Figure 4), whereas in the LIF-injected mice, there were significantly more Ki-67–positive cardiomyocytes (Figure 4).

It was recently reported that undifferentiated stem cells in the bone marrow may be transported to the heart by cytokines and differentiate into endothelial cells and cardiomyocytes.[7] We examined whether LIF stimulated the mobilization and differentiation of BMCs after MI. We transplanted BMCs isolated from GFP-transgenic mice into irradiated wild-type mice and induced MI in them. Two weeks after MI, there were a few GFP-positive cells in the border zone of the infarction in the vehicle-injected mice (data not shown). In the heart of LIF-injected mice, however, there were clusters of GFP-positive cells in certain areas (Figure 5B). Furthermore, there were more GFP-positive cardiomyocytes in the myocardium of LIF-injected mice than in that of vehicle-treated mice (Figure 5, C and D). Also, differentiation of BMCs into cardiomyocytes was confirmed by use of immu-
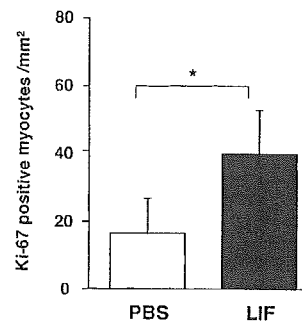
nostaining for cTnT followed by Y chromosome FISH. After 2 weeks of MI, positive signals for Y chromosome were observed in the myocardium of LIF-injected female recipients that had received transplants of male BMCs (Figure 5E). More GFP-positive capillaries were also observed in the border zone of the infarcted heart of LIF cDNA–treated mice (PBS-treated, $11\pm4/mm^2$; LIF-treated, $23\pm3/mm^2$; $P<0.05$) (Figure 5F). These results collectively suggest that LIF induced mobilization and differentiation of BMCs into cardiomyocytes and vascular endothelial cells.

Discussion

LIF has potent effects on various cellular events such as proliferation, differentiation, and survival of many cells.[10,16,18,34–36] Activation of gp130 by LIF activates several pathways, including the Jak/STAT-3, phosphoinositide-3′-kinase (PI3K)/Akt, and Ras/ERK pathways.[18,35,37] Activation of the Jak/STAT-3 pathway has been reported to induce upregulation of antiapoptosis proteins such as Bcl-2, Bcl-xl, nuclear factor-κB, and SOCS.[35] Activation of the PI3K/Akt and Ras/ERK pathways has been reported to enhance survival of many types of cells.[18,37] The activation of these pathways in the heart may prevent cardiomyocytes from death in MI. Neovascularization is important to prevent further cell death and improve cardiac function during LV remodeling after MI.[33,38] Activation of STAT-3 has been reported to enhance neovascularization in the myocardium through enhanced expression of VEGF.[28] Our results also showed that LIF suppresses cardiomyocyte death and increases vasculature in the border zone of infarcted hearts through enhanced expression of VEGF.

Although cardiomyocytes have long been thought to be terminally differentiated and do not undergo mitosis after birth, it was recently reported that even adult mammalian cardiomyocytes can divide.[3,33,39] However, their proliferative ability is so limited that the large infarcted area with fibrotic tissue results in cardiac dysfunction. The IL-6 family of cytokines has been reported to induce proliferation of many types of cells,[9] and the results of knockout and dominant negative experiments suggest that gp130 is involved in the growth and proliferation of cardiomyocytes.[15,17] It is interest-
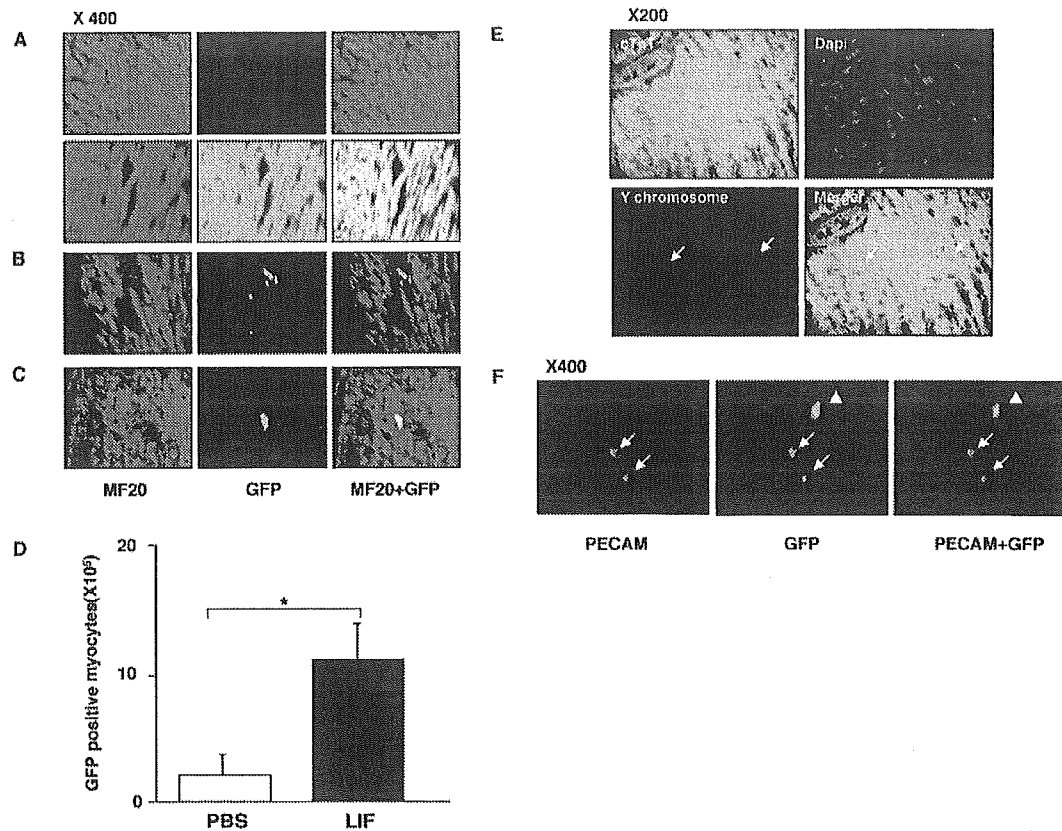
Figure 5. Mobilization and differentiation of BMCs 2 weeks after MI. A, Representative staining of hearts from wild-type (top) and GFP-transgenic mice (bottom). B, GFP-positive cells in MI heart of LIF cDNA-injected mice. BMCs formed clusters in some areas of border zone. C, MI heart of LIF cDNA-injected mice. A GFP-positive cardiomyocyte was observed in border zone. Red fluorescence indicates cardiac myosin; green fluorescence indicates GFP-positive cells; yellow labeling indicates cardiomyocyte derived from GFP-positive cells. A–C, Left, stained with MF20 (anti-myosin antibody); middle, GFP; right, merge. D, Number of GFP-positive cardiomyocytes. Cardiomyocytes were counted in whole LVFW area for each section. Twenty sections from each heart were measured. Values are expressed as number of GFP-positive cardiomyocytes per 10^5 cardiomyocytes. Data are shown as mean ± SD of 3 mice. *$P<0.05$. E, Representative FISH for murine Y chromosome and immunostaining for cTnT in border zone. Staining: green, cTnT; blue, DAPI for nuclear chromatin; red, rhodamine for Y chromosome. Cardiomyocyte nuclei contain Y chromosomes (arrows), indicative of BMC origin. F, Representative staining of GFP-positive microvessels in border zone. Red fluorescence indicates staining of PECAM; green fluorescence indicates GFP-positive cells; yellow labeling indicates newly formed vessels derived from GFP-positive cells (arrows). Arrowheads show a GFP-positive cell unlabeled by PECAM.

ing to note that there were many cardiomyocytes that expressed Ki-67 in the ischemic zone as well as in the border zone in LIF-injected mice. Although it remains to be determined how many cardiac myocytes are increased, LIF-induced proliferation of cardiomyocytes may contribute, at least in part, to the increase in cardiomyocytes in the ischemic area of MI hearts.

Recently, BMCs have been reported to differentiate into cardiomyocytes after MI.[5,6,8] It has also been suggested that pretreatment with stem-cell factor and granulocyte-colony–stimulating factor promoted the mobilization of BMCs into the myocardium and their differentiation into cardiomyocytes after induction of MI.[7] Here, we also provide evidence that LIF induces not only mobilization of BMCs to myocardium but also differentiation of BMCs into cardiomyocytes after MI. Although LIF inhibits differentiation and maintains stem-cell renewal of embryonic stem cells in vitro,[22] LIF induces differentiation of many cell types.[11–14,40] The bidirec-

tional effects of LIF on differentiation are dependent on the cell lineages and stages of differentiation.[40]

LIF protected cardiac myocytes from death and enhanced neovascularization after MI. LIF also induced an increase in cardiomyocytes that are in the cell cycle. Moreover, LIF promoted mobilization of BMCs into the myocardium and their differentiation into cardiomyocytes. These pleiotropic effects of LIF may contribute to attenuating the extension of infarction and improve cardiac function. It was recently reported that adult humans have extracardiac progenitor cells that mobilize into and regenerate damaged myocardium at very low levels.[41] It remains to be determined whether LIF gene therapy promotes this process after MI in humans.

Acknowledgments

References

1. Anversa P, Cheng W, Liu Y, et al. Apoptosis and myocardial infarction. *Basic Res Cardiol.* 1998;3:8–12.
2. Anversa P, Kajstura J. Ventricular myocytes are not terminally differentiated in the adult mammalian heart. *Circ Res.* 1998;83:1–14.
3. Beltrami AP, Urbanek K, Kajstura J, et al. Evidence that human cardiac myocytes divide after myocardial infarction. *N Engl J Med.* 2001;344: 1750–1757.
4. Makino S, Fukuda K, Miyoshi S, et al. Cardiomyocytes can be generated from marrow stromal cells in vitro. *J Clin Invest.* 1999;103:697–705.
5. Orlic D, Kajstura J, Chimenti S, et al. Exogenous hematopoietic stem cells can regenerate infarcted myocardium. *Circulation.* 2000;102: 2672-g. Abstract.
6. Orlic D, Kajstura J, Chimenti S, et al. Bone marrow cells regenerate infarcted myocardium. *Nature.* 2001;410:701–705.
7. Orlic D, Kajstura J, Chimenti S, et al. Mobilized bone marrow cells repair the infarcted heart, improving function and survival. *Proc Natl Acad Sci U S A.* 2001;98:10344–10349.
8. Toma C, Pittenger MF, Cahill KS, et al. Human mesenchymal stem cells differentiate to a cardiomyocyte phenotype in the adult murine heart. *Circulation.* 2002;105:93–98.
9. Taga T, Kishimoto T. Gp130 and the interleukin-6 family of cytokines. *Annu Rev Immunol.* 1997;15:797–819.
10. Taupin JL, Pitard V, Dechanet J, et al. Leukemia inhibitory factor: part of a large ingathering family. *Int Rev Immunol.* 1998;16:397–426.
11. Husmann I, Soulet L, Gautron J, et al. Growth factors in skeletal muscle regeneration. *Cytokine Growth Factor Rev.* 1996;7:249–258.
12. Finkelstein DI, Bartlett PF, Horne MK, et al. Leukemia inhibitory factor is a myotrophic and neurotrophic agent that enhances the reinnervation of muscle in the rat. *J Neurosci Res.* 1996;46:122–128.
13. Michalopoulos GK, DeFrances MC. Liver regeneration. *Science.* 1997; 276:60–66.
14. Dazai S, Akita S, Hirano A, et al. Leukemia inhibitory factor enhances bone formation in calvarial bone defect. *J Craniofac Surg.* 2000;11: 513–520.
15. Yoshida K, Taga T, Saito M, et al. Targeted disruption of gp130, a common signal transducer for the interleukin 6 family of cytokines, leads to myocardial and hematological disorders. *Proc Natl Acad Sci U S A.* 1996;93:407–411.
16. Hirota H, Chen J, Betz UA, et al. Loss of a gp130 cardiac muscle cell survival pathway is a critical event in the onset of heart failure during biomechanical stress. *Cell.* 1999;97:189–198.
17. Uozumi H, Hiroi Y, Zou Y, et al. gp130 plays a critical role in pressure overload-induced cardiac hypertrophy. *J Biol Chem.* 2001;276: 23115–23119.
18. Negoro S, Oh H, Tone E, et al. Glycoprotein 130 regulates cardiac myocyte survival in doxorubicin-induced apoptosis through phosphatidylinositol 3-kinase/Akt phosphorylation and Bcl-xL/caspase-3 interaction. *Circulation.* 2001;103:555–561.
19. Pennica D, King KL, Shaw KJ, et al. Expression cloning of cardiotrophin 1, a cytokine that induces cardiac myocyte hypertrophy. *Proc Natl Acad Sci U S A.* 1995;92:1142–1146.
20. Kodama H, Fukuda K, Pan J, et al. Leukemia inhibitory factor, a potent cardiac hypertrophic cytokine, activates the JAK/STAT pathway in rat cardiomyocytes. *Circ Res.* 1997;81:656–663.
21. Harada K, Sugaya T, Murakami K, et al. Angiotensin II type 1A receptor knockout mice display less left ventricular remodeling and improved survival after myocardial infarction. *Circulation.* 1999;100:2093–2099.
22. Niwa H, Burdon T, Chambers I, et al. Self-renewal of pluripotent embryonic stem cells is mediated via activation of STAT3. *Genes Dev.* 1998;12:2048–2060.
23. Okabe M, Ikawa M, Kominami K, et al. "Green mice" as a source of ubiquitous green cells. *FEBS Lett.* 1997;407:313–319.
24. Morshead CM, Benveniste P, Iscove NN, et al. Hematopoietic competence is a rare property of neural stem cells that may depend on genetic and epigenetic alterations. *Nat Med.* 2002;8:268–273.
25. Bishop CE, Hatat D. Molecular cloning and sequence analysis of a mouse Y chromosome RNA transcript expressed in the testis. *Nucleic Acids Res.* 1987;15:2959–2969.
26. Guillen I, Blanes M, Gomez LM, et al. Cytokine signaling during myocardial infarction: sequential appearance of IL-1 beta and IL-6. *Am J Physiol.* 1995;269:R229–R235.
27. Pudil R, Pidrman V, Krejsek J, et al. Cytokines and adhesion molecules in the course of acute myocardial infarction. *Clin Chim Acta.* 1999;280: 127–134.
28. Osugi T, Oshima Y, Fujio Y, et al. Cardiac-specific activation of signal transducer and activator of transcription 3 promotes vascular formation in the heart. *J Biol Chem.* 2002;277:6676–6681.
29. Muller AM, Hermanns MI, Skrzynski C, et al. Expression of the endothelial markers PECAM-1, vWf, and CD34 in vivo and in vitro. *Exp Mol Pathol.* 2002;72:221–229.
30. Shih SC, Robinson GS, Perruzzi CA, et al. Molecular profiling of angiogenesis markers. *Am J Pathol.* 2002;161:35–41.
31. Thompson JA, Anderson KD, DiPietro JM, et al. Site-directed neovessel formation in vivo. *Science.* 1988;241:1349–1352.
32. Scholzen T, Gerdes J. The Ki-67 protein: from the known and the unknown. *J Cell Physiol.* 2000;182:311–322.
33. Anversa P, Nadal GB. Myocyte renewal and ventricular remodelling. *Nature.* 2002;415:240–243.
34. Pennica D, Arce V, Swanson TA, et al. Cardiotrophin-1, a cytokine present in embryonic muscle, supports long-term survival of spinal motoneurons. *Neuron.* 1996;17:63–74.
35. Hirano T, Ishihara K, Hibi M. Roles of STAT3 in mediating the cell growth, differentiation and survival signals relayed through the IL-6 family of cytokine receptors. *Oncogene.* 2000;19:2548–2556.
36. Butzkueven H, Zhang JG, Soilu HM, et al. LIF receptor signaling limits immune-mediated demyelination by enhancing oligodendrocyte survival. *Nat Med.* 2002;8:613–619.
37. Yasukawa H, Hoshijima M, Gu Y, et al. Suppressor of cytokine signaling-3 is a biomechanical stress-inducible gene that suppresses gp130-mediated cardiac myocyte hypertrophy and survival pathways. *J Clin Invest.* 2001;108:1459–1467.
38. Isner JM. Myocardial gene therapy. *Nature.* 2002;415:234–239.
39. Kajstura J, Leri A, Finato N, et al. Myocyte proliferation in end-stage cardiac failure in humans. *Proc Natl Acad Sci U S A.* 1998;95: 8801–8805.
40. Boeuf H, Merienne K, Jacquot S, et al. The ribosomal S6 kinases, cAMP-responsive element-binding, and STAT3 proteins are regulated by different leukemia inhibitory factor signaling pathways in mouse embryonic stem cells. *J Biol Chem.* 2001;276:46204–46211.
41. Laflamme MA, Myerson D, Saffitz JE, et al. Evidence for cardiomyocyte repopulation by extracardiac progenitors in transplanted human hearts. *Circ Res.* 2002;90:634–640.

ELSEVIER

Original Article

3-Hydroxy-3-methylglutaryl coenzyme A reductase inhibitors prevent the development of cardiac hypertrophy and heart failure in rats

Hiroshi Hasegawa, Rie Yamamoto, Hiroyuki Takano, Miho Mizukami,
Masayuki Asakawa, Toshio Nagai, Issei Komuro *

*Department of Cardiovascular Science and Medicine, Chiba University Graduate School of Medicine (M4),
1-8-1 Inohana, Chuo-ku, Chiba 260-8670, Japan*

Abstract

Objectives. – The aim of the present study was to determine whether 3-hydroxy-3-methylglutaryl coenzyme A reductase inhibitors (statins) have preventive effects on the development of cardiac hypertrophy and heart failure.

Background. – Statins have been reported to have various pleiotropic effects, such as inhibition of inflammation and cell proliferation.

Methods. – Dahl rats were divided into three groups: LS, the rats fed the low-salt diet (0.3% NaCl); HS, the rats fed the high-salt diet (8% NaCl) from the age of 6 weeks; and CERI, the rats fed the high-salt diet with cerivastatin 1 mg/kg/d by gavage from the age of 6 weeks

Results. – In HS rats, cardiac function was markedly impaired and all rats showed the signs of heart failure within 17 weeks of age. In CERI rats, cardiac function was better than that of HS and no rats were dead up to 17 weeks of age. The development of cardiac hypertrophy and fibrosis was attenuated, and the number of apoptotic cells and expression of proinflammatory cytokine interleukin (IL)-1β gene were less as compared with HS rats. Pretreatment of cerivastatin suppressed the adriamycin-induced apoptosis of cultured cardiomyocytes of neonatal rats.

Conclusions. – These results suggest that statins have a protective effect on cardiac myocytes and may be useful to prevent the development of hypertensive heart failure.

© 2003 Elsevier Ltd. All rights reserved.

Keywords: Apoptosis; Fibrosis; Heart failure; Hypertrophy; Statin; Salt-sensitive rat; TUNEL; Interleukin-1β

1. Introduction

Hypertension causes left ventricular (LV) hypertrophy. Although LV hypertrophy is formed in response to hemodynamic overload to normalize wall stress [1], prolonged LV hypertrophy may result in cardiac dysfunction leading to subsequent cardiovascular events, such as congestive heart failure (CHF) and sudden death [2]. Despite numerous studies on cardiac hypertrophy and CHF, the precise mechanisms of the transition from LV hypertrophy to CHF are not fully

understood [3]. CHF is a complex syndrome that consists not only of cardiac dysfunction but also of metabolic and neuro-humoral alterations [4]. In particular, cytokines have recently attracted great attention as a cause of CHF. Proinflammatory cytokines, such as interleukin (IL)-1β and tumor necrosis factor (TNF)-α, have been reported to have a negative-inotropic effect on the perfused heart or cultured myocytes via NO-dependent or -independent mechanisms [5,6]. IL-1β also induces hypertrophy of cultured myocytes associated with the induction of fetal gene program [7].

3-Hydroxy-3-methylglutaryl coenzyme A (HMG-CoA) reductase inhibitors, so-called statins, are widely used to lower plasma cholesterol levels and decrease the incidence of myocardial infarction and ischemic stroke [8–10]. It has been recently reported that the beneficial effects of statins on coronary heart disease (CHD) are not limited to their ability to lower plasma cholesterol levels [11], but statins exhibit various pleiotropic effects on atherosclerosis including reduction of plaque thrombogenicity, inhibition of cellular

proliferation and migration, and improvement of endothelial function [10]. The inflammatory process has been reported to be involved in atherosclerosis and statins inhibit the production of inflammatory cytokines, such as IL-1β, in endothelium [12].

The Dahl salt-sensitive (DS) rat develops systemic hypertension with a high-salt diet and shows concentric LV hypertrophy and CHF [13,14]. Vasoactive peptides, such as endothelin-1 and angiotensin II, in the heart are thought to have deleterious effects on the development of CHF in this model [15,16]. Moreover, it has been reported that in DS rats, the expression of cytokines is increased in the hypertrophied heart and that the expression levels become more pronounced when CHF develops [17]. The aim of this study is to determine whether statins prevent the development of cardiac hypertrophy and the transition from hypertrophy to CHF using DS heart failure model.

2. Methods

2.1. Materials

Cerivastatin and adriamycin (ADR) were generous gifts from Bayer pharmaceutical (Osaka, Japan) and Kyowa Hakko Kogyo Co. Ltd. (Tokyo, Japan), respectively.

2.2. Animals and experimental protocol

Male DS rats of 5-week-old were obtained from SLC (Shizuoka, Japan). All rats were housed in climate-controled metabolic cages with a 12:12-h light–dark cycle. The rats were fed a diet containing 0.3% NaCl until the age of 6 weeks and they were fed a diet containing 8% NaCl (MF, Oriental yeast, Tokyo, Japan) from 6 weeks of age throughout the experiment [13]. Seven out of 22 rats were given cerivastatin (1 mg/kg/d) by gavage once a day from 6 to 17 weeks. Blood pressure and body weight of each animal were measured every week. The peak systolic pressure was recorded by a photoelectric pulse device (Softron BP-98A, Softron Co, Japan) placed on the tail of unanesthetized rats as described previously [18]. Five rats were fed a diet containing 0.3% NaCl throughout this experiment as a normal blood pressure control. DS rats with CHF were sacrificed at 17 weeks, before their natural death, when signs of CHF, such as rapid and labored respiration, and LV diffuse hypokinesis on echocardiography, were observed. Six-week-old DS rats, 11-week-old DS rats and DS rats with CHF (17-week-old) were studied. Throughout the studies, all animals were treated humanly in accordance with the guidelines on animal experimentation of our institute and the American Heart Association on Research Animal Use (*Circulation*, April 1995).

2.3. Histological analysis

After the heart was removed, the heart was weighed, fixed in 3.8% with perfusion of formaldehyde, embedded in paraf-

fin, sectioned into 4 μm slices, and stained with hematoxylin–eosin (H–E) staining or van Gieson staining [18]. To determine the degree of collagen fiber accumulation, we selected 10 fields at random and calculated the ratio of van Gieson staining fibrosis area to total myocardium area with the software NIH IMAGE (NIH, Research Service Branch) for image analysis [18]. For the detection of apoptotic cells, the *in situ* terminal deoxynucleotidyl transfer-mediated end labeling of fragmented nuclei assay (TUNEL) and immunohistochemical analysis to detect active caspase-3 were performed using an in situ apoptosis detection kit (CardioTACS™, TREVIGEN, Inc.) and anti-active caspase-3 polyclonal antibody (Promega, Madison, USA), respectively, according to the supplier's instructions. A part of the LV was frozen at −80 °C for mRNA analysis.

2.4. Echocardiography

Transthoracic echocardiography was performed at the age of 6, 11, 17 weeks of all rats with the HP Sonos 100 (Hewlett-Packard Co) with a 10-MHz imaging linear scan probe transducer as described previously [18]. For DS rats, the final echocardiography was taken just before death, when labored respiration became apparent. We determined the LV end-diastolic diameter (LVEDd) as the widest and the end-systolic diameter (LVEDs) as the narrowest dimension in the M-mode recordings. The LV posterior wall thickness (LVPWT) was measured at the time of LVEDd measurement. LV fractioning shortening (FS) and the LV mass were calculated according to the following formulas [13]:

$$LV\ FS\ (\%) = (LVEDd - LVEDs)/LVEDd \times 100$$
$$LV\ mass\ g = 1.05 \times LVEDd + 2 \times LVPWT3 - LVEDd3$$

2.5. Quantitative analysis of RNA content

Total RNA was isolated from rat heart ventricle using lithium/urea methods and separated on a 1.0% agarose/formaldehyde gel. cDNA of BNP was labeled by a random priming method with [α-^{32}P]dCTP and hybridized to membranes as described previously [18]. RNA protection assay (using 20 μg of total RNA) was done using rat cytokine Multi-Probe Template Set (BD Pharmingen Bioscience) according to technical data sheet. Hybridized bands were quantified with FUJIX Bio-Imaging Analyzer BAS 2000 (Fuji film Co, Japan).

2.6. Cell viability assay using rat neonatal cardiomyocyte

Cardiomyocytes of neonatal rats were prepared by a modified [19] method of Simpson [20]. Cardiomyocytes were plated at a density of 5 × 10⁵ cells/cm² on 35-mm culture dishes (Falcon Primaria) or on glass slips with minimum essential medium Eagle (MEM, M4655) containing 5% iron-fortified calf serum (CS, JRH biosciences). At 24 h after seeding, the culture medium was changed to MEM with 0.5% CS. After 24 h, ADR were added and incubated for 16 h

with or without pretreatment of cerivastatin for 1 h. To detect TUNEL-positive cells, *in situ* Apoptosis Detection Kit (TaKaRa Biomedicals, Japan) was used.

2.7. Statistical analysis

All data are expressed as mean ± S.E.M. of three to four independent experiments in each instance. Mean difference among three groups was tested by one-way ANOVA followed by Scheffe's modified *F*-test for multiple comparisons. Comparisons from follow-up body weight, blood pressure, pulse rate, and echocardiographic data were tested using repeated measure ANOVA followed by Scheffe's modified *F*-test. The significance of the difference between group means was analyzed by Student's *t*-test. Values of $P < 0.05$ were considered statistically significant.

3. Results

3.1. Life span of DS rats

DS rats were divided into three groups: LS, the DS rats fed the low-salt diet (0.3% NaCl); HS, the DS rats fed the high-salt diet (8% NaCl) from the age of 6 weeks; and CERI, the DS rats fed the high-salt diet and treated with cerivastatin by gavage from the age of 6 weeks (1 mg/kg/d). There were no significant differences in physiological parameters, such as body weight, heart rate and blood pressure, and in echocardiographic parameters including intraventricular septal thickness and posterior wall thickness at the start point among these groups (Fig. 1, Table 1). Blood pressure was gradually increased, reached the level of over 230 mmHg by the 11 weeks old, and remained elevated over 200 mmHg thereafter in both HS and CERI rats. There was no significant difference in blood pressure between HS and CERI rats (Fig. 1). At the age of 14–16 weeks, all HS rats lost body weight and displayed rapid and labored respiration characteristic of CHF and five rats out of 10 were dead by 17 weeks of
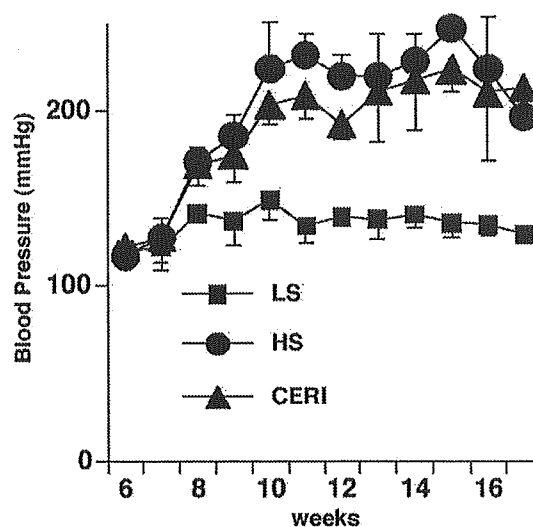

Fig. 1. The change of blood pressure. Blood pressure in LS, HS, and CERI rats. Data are expressed as mean ± S.E.M. (n = 5, 10, and 7 in LS (closed square), HS (closed circle), and CERI (closed triangle) rats).

age. On the other hand, all LS and CERI group rats were alive without any symptoms.

3.2. Cardiac hypertrophy and LV dilatation

HS rats developed remarkable cardiac hypertrophy compared with LS rats (the heart weight to body weight (H/B) ratio of 17-week-old LS, 2.82 ± 0.14 vs. HS, 5.82 ± 0.20, $P < 0.01$) (Fig. 2A,B,D). The increase in the H/B ratio was attenuated significantly in CERI group compared with HS group (CERI, 4.18 ± 0.22, $P < 0.01$ vs. HS) (Fig. 2C,D). We assessed the wall thickness, LV-dimension and cardiac function by echocardiography (Table 1). At the age of 11 and 17 weeks, the LVPWT diameter was increased in the HS rats compared with LS rats, and treatment with cerivastatin significantly suppressed the thickening of LV wall. LVEDd of HS rats of 17-week old was significantly larger than that of

Table 1
Serial measurements of echocardiography in LS, HS, and CERI rats

	BW (g)	LVPWT (mm)	LVEDd (mm)	LVEDs (mm)	FS (%)	LV mass (g)
LS rats						
6 weeks	190 ± 3.2	1.41 ± 0.06	4.91 ± 0.30	2.60 ± 0.36	48.2 ± 2.48	0.52 ± 0.03
11 weeks	373 ± 5.1	1.61 ± 0.05	7.12 ± 0.28	4.15 ± 0.29	42.0 ± 1.99	0.79 ± 0.03
17 weeks	446 ± 6.5	1.60 ± 0.04	7.42 ± 0.43	4.37 ± 0.49	41.3 ± 3.40	0.83 ± 0.09
HS rats						
6 weeks	190 ± 3.2	1.40 ± 0.05	5.01 ± 0.30	2.45 ± 0.18	45.8 ± 3.48	0.49 ± 0.04
11 weeks	315 ± 17.1	2.04 ± 0.04*	6.78 ± 0.09	3.75 ± 0.10	44.7 ± 1.05	1.02 ± 0.01*
17 weeks	310 ± 6.4*	2.07 ± 0.24*	9.25 ± 0.81*	6.96 ± 0.93*	25.0 ± 3.48*	1.69 ± 0.03*
CERI rats						
6 weeks	196 ± 3.6	1.40 ± 0.05	4.95 ± 0.56	2.75 ± 0.51	42.5 ± 3.01	0.48 ± 0.05
11 weeks	330 ± 3.8	1.85 ± 0.03*·**	6.91 ± 0.24	4.36 ± 0.26	40.1 ± 2.01	0.91 ± 0.02
17 weeks	362 ± 11.5*·**	1.85 ± 0.10*·**	7.37 ± 0.52**	4.53 ± 0.64**	38.7 ± 4.60 **	1.01 ± 0.11*·**

Data are expressed as mean ± SEM.
$*P < 0.05$ vs. age-matched LS rats.
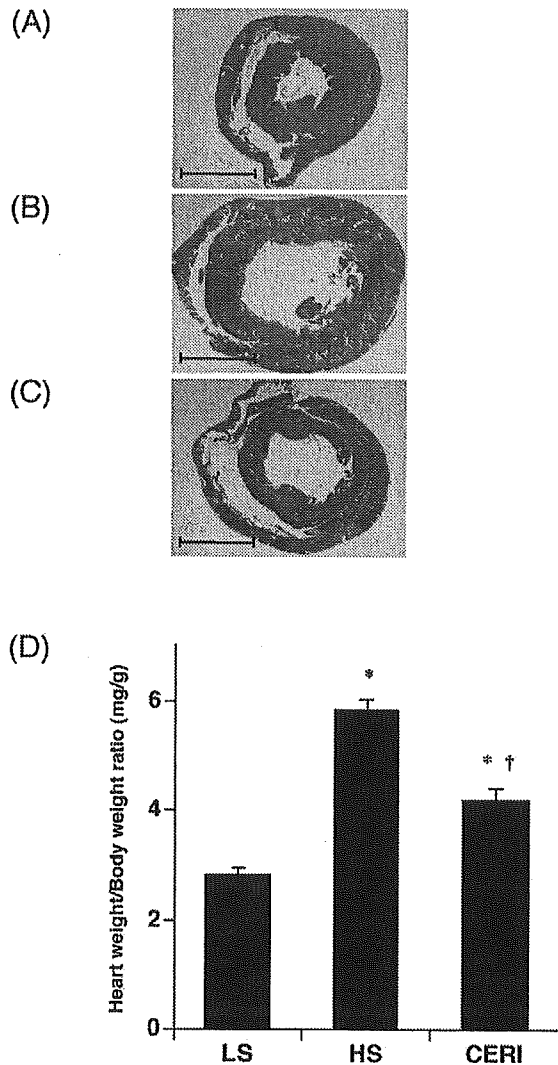$**P < 0.05$ vs. age-matched HS rats.

(A)

(B)

(C)

(D)

Fig. 2. The LV hypertrophy of DS rats at 17 weeks. H–E staining of LV tissue of (A) LS rats, (B) HS rats, and (C) CERI rats of 17-week old (magnification ×10; scale bar, 5 mm). (D) Treatment of cerivastatin significantly reduced cardiac hypertrophy at 17 weeks. The bar indicates the H/B ratio. Data are expressed as mean ± S.E.M. *$P < 0.01$ vs. LS rats. †$P < 0.01$ vs. HS rats.

LS rats and LVEDd of CERI rats was significantly smaller compared with that of HS rats. The LV mass calculated from the echocardiogram correlated well with the H/B ratio. The FS of LV wall was reduced in 17-week-old HS rats compared with LS rats, and treatment with cerivastatin significantly suppressed the reduction of FS and there was no significant difference between CERI and LS.

3.3. Histopathology of myocardial fibrosis

Marked cardiomyocyte hypertrophy and interstitial fibrosis were observed in the LV tissue of 17-week-old HS rats
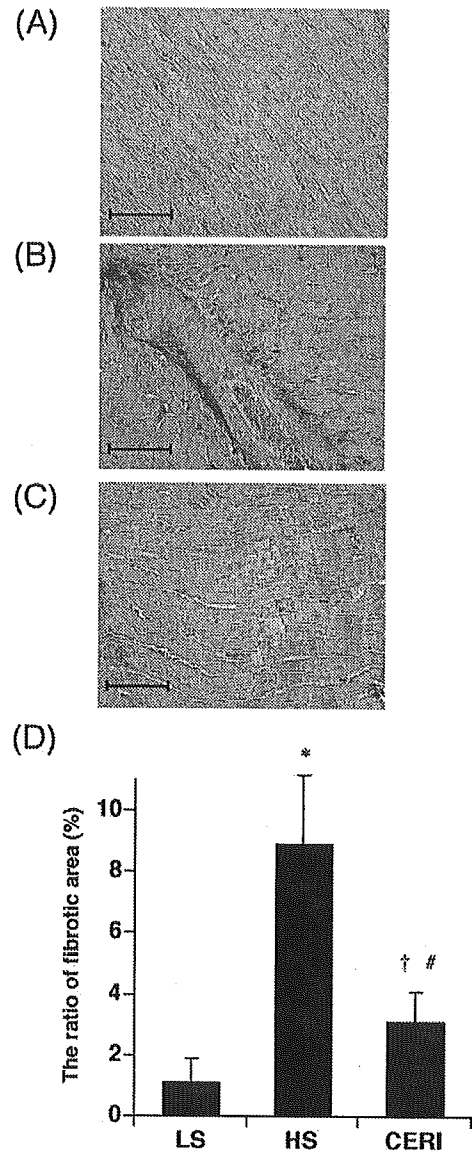
(A)

(B)

(C)

(D)

Fig. 3. Microscopic analysis of rats at 17 weeks. The van Gieson staining was performed on LV heart tissue of (A) LS rats, (B) HS rats, and (C) CERI rats of 17-week old (magnification ×200; scale bar, 100 μm). (D) The ratio of fibrotic area to total myocardium area was determined by van Gieson staining. Data are expressed as mean ± S.E.M. *$P < 0.01$ vs. LS rats. †$P < 0.05$ vs. LS rats. #$P < 0.05$ vs. HS rats.

compared to LS rats (Fig. 3A,B,D). Treatment with cerivastatin significantly inhibited the fibrosis as well as the LV hypertrophy (Fig. 3C,D). Quantitative analysis of myocardial fibrosis using van Gieson staining of the heart tissue revealed that there was a significant difference in fibrosis area between CERI and HS (LS, 1.1 ± 1.3; HS, 8.9 ± 3.9; CERI, 3.1 ± 1.7 %, HS vs. CERI, $P < 0.05$) (Fig. 3D).
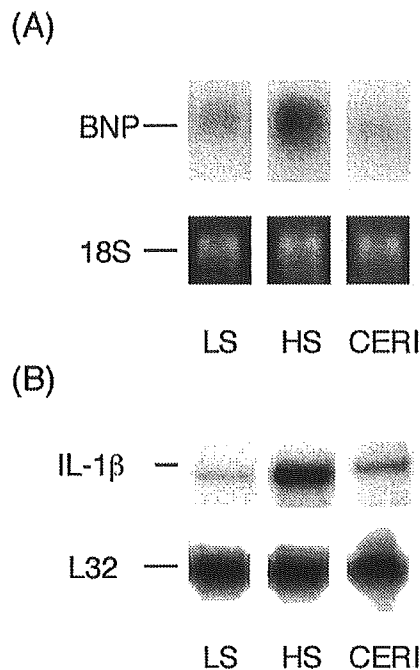
(A)

(B)

Fig. 4. Gene expression in the heart of rats at 17 weeks. (A) Representative autoradiography of northern blot analysis of BNP gene. Equal loading (10 µg) was confirmed by 18S ribosomal RNA density after ethidium bromide staining. (B) Representative autoradiography of IL-1β gene detected by RNA protection assay. Equal loading (20 µg) was confirmed by expression level of L32 gene.

3.4. Gene expression

The mRNA levels of brain natriuretic peptide (BNP) were significantly higher (~2.3-fold) in HS rats compared with LS rats (Fig. 4A). There was no significant difference in BNP mRNA levels between LS and CERI rats. The expression of IL-1β gene was markedly (~4.9-fold) increased in HS hearts compared with LS hearts, and treatment with cerivastatin significantly attenuated its increase (CERI, 2.2-fold compared with LS, $P < 0.05$ vs. HS).

3.5. Cell viability assay of cardiomyocytes

Cardiomyocyte apoptosis is also known to be an important cause of heart failure. Some of cellular nuclei showed positive for TUNELstaining in ventricular tissues of HS rats and treatment with cerivastatin inhibited it significantly (LS, 0 ± 0%; HS, 0.75 ± 0.20%; CERI, 0.24 ± 0.10%, CERI vs. HS, $P < 0.05$) (Fig. 5A). Moreover, the increased number of cells positive for active caspase-3 was significantly decreased in CERI rats compared to HS rats (LS, 0.0046 ± 0.0051%; HS, 0.46 ± 0.038%; CERI, 0.073 ± 0.024%, CERI vs. HS, $P < 0.01$) (Fig. 5B). Since it is difficult to distinguish cardiomyocytes from other cells including fibroblasts in these methods, we examined the effect of cerivastatin on ADR-induced cardiomyocyte apoptosis using cultured cardiac myocytes. The number of apoptotic cardiomyocytes is not
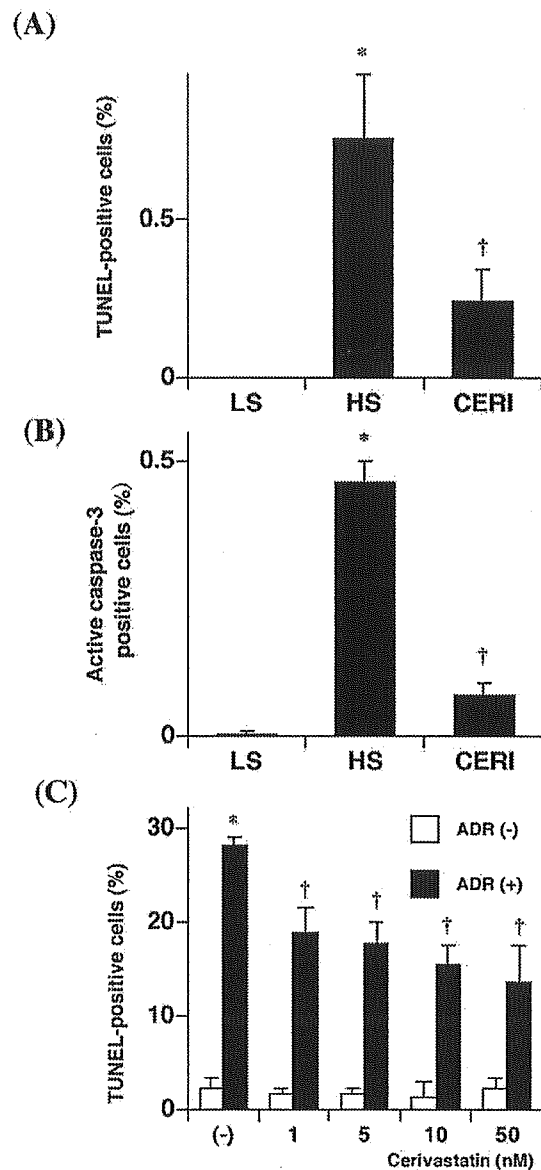
(A)

(B)

(C)

Fig. 5. Cardiomyocyte death. (A) The percentage of TUNEL-positive cells in the heart of rats at 17 weeks. Data are expressed as mean ± S.E.M. *$P < 0.01$ vs. LS rats. †$P < 0.05$ vs. HS rats. (B) The percentage of cells positive for active caspase-3 in the heart of rats at 17 weeks. Data are expressed as mean ± S.E.M. *$P < 0.01$ vs. LS rats. †$P < 0.01$ vs. HS rats. (C) Effects of cerivastatin on percentage of cultured cardiomyocytes undergoing apoptosis measured by TUNEL technique. The effects of each concentration of cerivastatin were determined with or without ADR. One hundred α-actinin-positive cardiomyocytes were counted, and the number of TUNEL-positive cells was presented as a percentage. Data are mean ±S.E.M. from three independent experiments. *$P < 0.01$ vs. ADR (–), cerivastatin (–). †$P < 0.01$ vs. ADR (+), cerivastatin (–).

changed by the treatment of cerivastatin without ADR treatment. A number of cardiomyocytes showed positive for TUNEL staining by the ADR treatment and many TUNEL-

positive cells had condensed nuclei, which are characteristic of apoptosis. The number of TUNEL-positive cardiomyocytes was significantly reduced with cerivastatin treatment dose dependently (Fig. 5C).

4. Discussion

Many factors have been reported to be involved in the transition from compensated cardiac hypertrophy to decompensated heart failure. They include abnormalities in calcium handling, apoptosis of cardiac myocytes, increases in cytokine expression and extracellular matrix, and activation of neurohumoral factors. The DS rat develops systemic hypertension, depending on the amount of sodium supplied in the diet [13], and cardiac hypertrophy with interstitial fibrosis. Prolonged hypertension induces reduced myocardial contraction and relaxation velocities [13,14], indicating that this model fully recapitulates the phenotype of human LV hypertrophy and hypertensive heart failure. Treatment with cerivastatin significantly reduced heart weight, LV wall thickness and LV diameter, and improved LV function. Increases in expression level of BNP and IL-1β gene were inhibited by cerivastatin treatment. In addition, cerivastatin prevented apoptosis in LV tissue of HS rats and in ADR-induced cultured cardiomyocytes.

The cerivastatin treatment inhibited the development of cardiac hypertrophy in DS rats. Statin-induced inhibition of cardiac hypertrophy has been reported in several models, such as angiotensin II-induced myocyte hypertrophy [21], pressure overload-induced LV hypertrophy [22], cardiac hypertrophy of human renin and angiotensinogen transgenic rats model [23], and transgenic rabbit model of hypertrophic cardiomyopathy [24]. Statins have been reported to inhibit the synthesis of isoprenoid intermediates of cholesterol biosynthesis, such as farnesylpyrophosphate and geranylpyrophosphate, which are important in the post-translational modification of the small GTP-binding protein Ras and Rho family proteins, respectively. This modification step is essential for maturation, membrane localization, and the subsequent activation of these small GTP-binding proteins. Rho family proteins have been reported to play an important role in the development of cardiac hypertrophy [25]. The treatment of statin inhibited the GTP-binding activity of Rho proteins and intracellular oxidation, and subsequently inhibited the cardiac development of hypertrophy induced by angiotensin II [26]. Inhibition of Rho kinase has been reported to attenuate LV hypertrophy and lung congestion [27]. These results and observations suggest that the inhibition of Rho kinase may be involved in the inhibitory mechanism of statins on hypertensive heart failure.

The proinflammatory cytokines, which act in an autocrine or paracrine manner, have been reported to be involved in the pathogenesis of myocarditis [28], dilated cardiomyopathy [29], and ischemic heart disease [30]. Proinflammatory cytokines (such as IL-1β and TNF-α) have a negative-inotropic effect on the perfused heart or cultured myocytes via NO-

dependent or -independent mechanisms [5,6]. IL-1β induces hypertrophy of cultured cardiomyocytes associated with the induction of fetal genes [7]. In this study, among various cytokines including IL-1α, IL-1β, IL-2, IL-3, IL-4, IL-5, IL-6, IL-10, TNF-α, TNF-β, and IFN-γ, only IL-1β was significantly upregulated in Dahl HS rats and the upregulation of IL-1β was inhibited by the treatment of cerivastatin. Although the expression of TNF-α was also upregulated in the heart of HS rats compared with LS rats, the treatment of cerivastatin did not significantly reduce its expression. The expression levels of other cytokines (such as IL-1α, IL-2, IL-3, IL-4, IL-5, IL-6, IL-10, TNF-β, and IFN-γ) were under detectable level in this study. We tried to examine the protein level of IL-1β but failed possibly because of small amount of IL-1β protein. IL-1β has a negative-inotropic effect [5,31] through suppressing Ca^{2+} current [32] and deleterious effect on myocyte metabolism [33], and promote fibrosis [34]. Since there is good correlation between IL-1β expression levels and the degree of cardiac hypertrophy and failure [17], IL-1β may be involved in the inhibitory mechanisms of cerivastatin on pathogenesis of cardiac hypertrophy and progression of hypertensive heart failure in DS rats.

In addition to necrosis, cardiomyocyte loss by apoptosis has recently been recognized as a potential cause of CHF [35]. Recently, it was reported that cardiomyocyte apoptosis is also a terminal event in the vicious cycle of heart failure in DS rats [36]. To examine whether treatment with cerivastatin inhibited the apoptosis of cardiac myocytes in vivo, we performed TUNEL analysis and immunohistochemical analysis to detect active caspase-3, a molecule involved in the final executional step of apoptosis [37]. Much more nuclei showed positive for TUNELstaining and expression of activated caspase-3 in the ventricle of DS rats than CERI rats, suggesting that a number of myocytes are undergoing an apoptotic death and that treatment of cerivastatin may rescue it. To confirm whether cerivastatin inhibits apoptosis of cardiomyocytes, we used in vitro assay system of ADR-induced cardiomyocyte death. Using these assays, we clearly showed that cerivastatin prevents apoptosis of cardiomyocytes. The prevention of cardiomyocyte apoptosis may be a mechanism of cerivastatin-induced inhibition of the development of heart failure. It was recently reported that fluvastatin, one of the hydrophobic statins, induced apoptosis in cultured neonatal cardiomyocytes [38]. In this study, however, cerivastatin did not induce cardiac apoptosis. The different effects of statins may come from the difference of statins used (cerivastatin in this study vs. fluvastatin in 38) or from the different dose of statins used. The anti-apoptotic effect of cerivastatin was observed at the concentration of 1 nM, which is clinical dose in humans (C_{max}; 3–8 nM). The concentration (3–10 μM) of fluvastatin they used seems to be very high, because clinical C_{max} of fluvastatin is about 0.3 μM.

The pleiotropic effects of statins have been reported on the vascular wall [9,10]. Most of these studies are focused on cell migration, proliferation, and regulation of nitric oxide synthesis. Lipophilic statins have an anti-inflammatory effect,

and they actually reduce the expression of mRNA levels of IL-1β in endothelial cells [12]. We demonstrated that one of lipophilic statins, cerivastatin, reduced the expression level of IL-1β in heart tissue of CHF rats. The increased expression of proinflammatory cytokines may play, in conjunction with other humoral factors, an important role in the development of cardiac hypertrophy and failure. IL-1β has been reported to induce apoptosis of cardiomyocytes [39] and fibrosis of ventricles [34] as well as cardiomyocyte hypertrophy [7]. The mechanism of the effect of statins to inhibit apoptosis and the expression of IL-1β in cardiomyocytes may be further examined. Hypertrophy, fibrosis and apoptosis are the major clinical and pathological phenotypes leading to heart failure. The present pharmacological treatments for the hypertensive heart failure are not sufficient, and statins may be useful to prevent the development of hypertensive heart failure.

In conclusion, using DS rats hypertensive heart failure model, we evaluated the cardioprotective effects of cerivastatin on cardiac hypertrophy and function. In HS rats, cardiac function was markedly impaired and all rats showed the signs of heart failure within 17 weeks of age. In rats treated with cerivastatin, cardiac function was better than that of HS without any treatment and no rats were dead up to 17 weeks of age. The development of cardiac hypertrophy and fibrosis was attenuated, and apoptosis of cardiomyocytes and expression of a proinflammatory cytokine IL-1β gene were less as compared with HS rats. Pretreatment of cerivastatin suppressed the ADR-induced apoptosis of cultured cardiomyocytes of neonatal rats. These results suggest that statins have a protective effect on cardiac myocytes and may be useful to prevent the development of hypertensive heart failure.

Acknowledgements

References

[1]   Frohlich ED. Cardiac hypertrophy in hypertension. N Engl J Med 1987;317:831–3.

[2]   Levy D, Garrison RJ, Savage DD, Kannel WB, Castelli WP. Prognostic implications of echocardiographically determined left ventricular mass in the Framingham Heart Study. N Engl J Med 1990;322:1561–6.

[3]   Katz AM. The cardiomyopathy of overload: an unnatural growth response in the hypertrophied heart. Ann Int Med 1994;121:363–71.

[4]   Tavi P, Laine M, Weckstrom M, Ruskoaho H. Cardiac mechanotransduction: from sensing to disease and treatment. Trends Pharmacol Sci 2001;22:254–60.

[5]   Finkel MS, Oddis CV, Jacob TD, Watkins SC, Hattler BG, Simmons RL. Negative inotropic effects of cytokines on the heart mediated by nitric oxide. Science 1992;257:387–9.

[6]   Schulz R, Panas DL, Catena R, Moncada S, Olley PM, Lopaschuk GD. The role of nitric oxide in cardiac depression induced by interleukin-1 beta and tumour necrosis factor-alpha. Br J Pharmacol 1995;114:27–34.

[7]   Thaik CM, Calderone A, Takahashi N, Colucci WS. Interleukin-1 beta modulates the growth and phenotype of neonatal rat cardiac myocytes. J Clin Invest 1995;96:1093–9.

[8]   Shepherd J, Cobbe SM, Ford I, Isles CG, Lorimer AR, MacFarlane PW, et al. Prevention of coronary heart disease with pravastatin in men with hypercholesterolemia. West of Scotland Coronary Prevention Study Group. N Engl J Med 1995;333:1301–7.

[9]   Takemoto M, Liao JK. Pleiotropic effects of 3-hydroxy-3-methylglutaryl coenzyme A reductase inhibitors. Arterioscler Thromb Vasc Biol 2001;21:1712–9.

[10] Vaughan CJ, Gotto Jr AM, Basson CT. The evolving role of statins in the management of atherosclerosis. J Am Coll Cardiol 2000;35:1–10.

[11] Scandinavian Simvastatin Survival Study Group. Randomised trial of cholesterol lowering in 4444 patients with coronary heart disease: the Scandinavian Simvastatin Survival Study (4S). Lancet 1994;344:1383–9.

[12] Inoue I, Goto S, Mizotani K, Awata T, Mastunaga T, Kawai S, et al. Lipophilic HMG-CoA reductase inhibitor has an anti-inflammatory effect: reduction of mRNA levels for interleukin-1beta, interleukin-6, cyclooxygenase-2, and p22phox by regulation of peroxisome proliferator-activated receptor alpha (PPARalpha) in primary endothelial cells. Life Sci 2000;67:863–76.

[13] Inoko M, Kihara Y, Morii I, Fujiwara H, Sasayama S. Transition from compensatory hypertrophy to dilated, failing left ventricles in Dahl salt-sensitive rats. Am J Physiol 1994;267(6 Pt 2):H2471–82.

[14] Inoko M, Kihara Y, Sasayama S. Neurohumoral factors during transition from left ventricular hypertrophy to failure in Dahl salt-sensitive rats. Biochem Biophys Res Commun 1995;206:814–20.

[15] Iwanaga Y, Kihara Y, Hasegawa K, Inagaki K, Yoneda T, Kaburagi S, et al. Cardiac endothelin-1 plays a critical role in the functional deterioration of left ventricles during the transition from compensatory hypertrophy to congestive heart failure in salt-sensitive hypertensive rats. Circulation 1998;98:2065–73.

[16] Iwanaga Y, Kihara Y, Inagaki K, Onozawa Y, Yoneda T, Kataoka K, et al. Differential effects of angiotensin II versus endothelin-1 inhibitions in hypertrophic left ventricular myocardium during transition to heart failure. Circulation 2001;104:606–12.

[17] Shioi T, Matsumori A, Kihara Y, Inoko M, Ono K, Iwanaga Y, et al. Increased expression of interleukin-1 beta and monocyte chemotactic and activating factor/monocyte chemoattractant protein-1 in the hypertrophied and failing heart with pressure overload. Circ Res 1997;81:664–71.

[18] Shimoyama M, Hayashi D, Zou Y, Takimoto E, Mizukami M, Monzen K, et al. Calcineurin inhibitor attenuates the development and induces the regression of cardiac hypertrophy in rats with salt-sensitive hypertension. Circulation 2000;102:1996–2004.

[19] Takano H, Nagai T, Asakawa M, Toyozaki T, Oka T, Komuro I, et al. Peroxisome proliferator-activated receptor activators inhibit lipopolysaccharide-induced tumor necrosis factor-alpha expression in neonatal rat cardiac myocytes. Circ Res 2000;87:596–602.

[20] Simpson P. Stimulation of hypertrophy of cultured neonatal rat heart cells through an alpha 1-adrenergic receptor and induction of beating through an alpha 1- and beta 1-adrenergic receptor interaction. Evidence for independent regulation of growth and beating. Circ Res 1985;56:884–94.

[21] Oi S, Haneda T, Osaki J, Kashiwagi Y, Nakamura Y, Kawabe J, et al. Lovastatin prevents angiotensin II-induced cardiac hypertrophy in cultured neonatal rat heart cells. Eur J Pharmacol 1999;376:139–48.

[22] Luo JD, Zhang WW, Zhang GP, Guan JX, Chen X. Simvastatin inhibits cardiac hypertrophy and angiotensin-converting enzyme activity in rats with aortic stenosis. Clin Exp Pharmacol Physiol 1999;26:903–8.

[23] Dechend R, Fiebeler A, Park JK, Muller DN, Theuer J, Mervaala E, et al. Amelioration of angiotensin II-induced cardiac injury by a 3-hydroxy-3-methylglutaryl coenzyme A reductase inhibitor. Circulation 2001;104:576–81.

[24] Patel R, Nagueh SF, Tsybouleva N, Abdellatif M, Lutucuta S, Kopelen HA, et al. Simvastatin induces regression of cardiac hypertrophy and fibrosis and improves cardiac function in a transgenic rabbit model of human hypertrophic cardiomyopathy. Circulation 2001;104:317–24.

[25] Sah VP, Hoshijima M, Chien KR, Brown JH. Rho is required for Galphaq and alpha1-adrenergic receptor signaling in cardiomyocytes. Dissociation of Ras and Rho pathways. J Biol Chem 1996;271:31185–90.

[26] Takemoto M, Node K, Nakagami H, Liao Y, Grimm M, Takemoto Y, et al. Statins as antioxidant therapy for preventing cardiac myocyte hypertrophy. J Clin Invest 2001;108:1429–37.

[27] Kobayashi N, Horinaka S, Mita S, Nakano S, Honda T, Yoshida K, et al. Critical role of rho-kinase pathway for cardiac performance and remodeling in failing rat hearts. Cardiovasc Res 2002;55:757–67.

[28] Shioi T, Matsumori A, Sasayama S. Persistent expression of cytokine in the chronic stage of viral myocarditis in mice. Circulation 1996;94:2930–7.

[29] Tsutamoto T, Wada A, Matsumoto T, Maeda K, Mabuchi N, Hayashi M, et al. Relationship between tumor necrosis factor-alpha production and oxidative stress in the failing hearts of patients with dilated cardiomyopathy. J Am Coll Cardiol 2001;37:2086–92.

[30] Plutzky J. Inflammatory pathways in atherosclerosis and acute coronary syndromes. Am J Cardiol 2001;88:10K–5K.

[31] Balligand JL, Ungureanu-Longrois D, Simmons WW, Pimental D, Malinski TA, Kapturczak M, et al. Cytokine-inducible nitric oxide synthase (iNOS) expression in cardiac myocytes. Characterization and regulation of iNOS expression and detection of iNOS activity in single cardiac myocytes in vitro. J Biol Chem 1994;269:27580–8.

[32] Liu S, Schreur KD. G protein-mediated suppression of L-type Ca^{2+} current by interleukin-1 beta in cultured rat ventricular myocytes. Am J Physiol 1995;268(2 Pt 1):C339–49.

[33] Hosenpud JD. The effects of interleukin 1 on myocardial function and metabolism. Clin Immunol Immunopathol 1993;68:175–80.

[34] Hinglais N, Heudes D, Nicoletti A, Mandet C, Laurent M, Bariety J, et al. Colocalization of myocardial fibrosis and inflammatory cells in rats. Lab Invest 1994;70:286–94.

[35] Kang PM, Izumo S. Apoptosis and heart failure: a critical review of the literature. Circ Res 2000;86:1107–13.

[36] Ikeda S, Hamada M, Qu P, Hiasa G, Hashida H, Shigematsu Y, et al. Relationship between cardiomyocyte cell death and cardiac function during hypertensive cardiac remodelling in Dahl rats. Clin Sci 2002;102:329–35.

[37] Martin SJ, Green DR. Protease activation during apoptosis: death by a thousand cuts? Cell 1995;82:349–52.

[38] Ogata Y, Takahashi M, Takeuchi K, Ueno S, Mano H, Ookawara S, et al. Fluvastatin induces apoptosis in rat neo natal cardiac myocytes: a possible mechanism of statin-attenuated cardiac hypertrophy. J Cardiovasc Pharmacol 2002;40:907–15.

[39] Pulkki KJ. Cytokines and cardiomyocyte death. Ann Med 1997;29:339–43.

A further understanding of the role of telomerase and telomere function would provide new insights into the treatment of human vascular disorders.

The Role of Telomerase Activation in the Regulation of Vascular Smooth Muscle Cell Proliferation

by *Tohru Minamino*
and *Issei Komuro*

Summary
Telomeres are primarily controlled by a highly specialized DNA polymerase, termed telomerase. In early studies, high levels of telomerase activity were detected in cancer cells, but no activity was found in most normal somatic cells, leading to the speculation that telomerase might be required for tumor growth. Recent studies have demonstrated that introduction of the telomerase catalytic component (TERT) into telomerase-negative cells activates telomerase and extends cell lifespan, whereas mice lacking telomerase activity revealed impaired cell proliferation in some organs as well as reduced tumorigenesis. These findings suggest that telomerase plays an important role in long-term cell viability and cell proliferation. We have recently demonstrated a crucial role of telomerase activation in the regulation of vascular smooth muscle cell (VSMC) proliferation and clarified the mechanisms by which telomerase is activated in the process of VSMC growth. Moreover, increasing evidence suggests that telomerase activity contributes to the vascular pathophysiology. Thus, further understanding of the role of telomerase and telomere function would provide new insights into the treatment of human vascular disorders. © 2003 Prous Science. All rights reserved.

Telomeres consist of repeats of sequence TTAGGG at the end of chromosomes. These DNA repeats are synthesized by enzymatic activity associated with an RNA protein complex called telomerase.[1] In most somatic cells, telomerase activity is undetectable, and telomere length decreases with increasing cell division. In contrast, in most cancer cells, telomeres stop shortening because of *de novo* synthesis of telomeric DNA by activated telomerase. Inhibition of telomerase has been shown to induce growth inhibition in cultured cancer cells.[2] Thus, telomerase activation has been implicated in tumorigenesis. Mice lacking telomerase RNA have been established and reported to show not only reduced tumorigenesis but also decreased cell proliferation in highly proliferative organs, suggesting that telomerase activity may be involved in the regulation of cell proliferation in normal somatic cells as well.[3,4] However, little is known about the role of telomere and telomerase activity in vascular cells until recently. In this article, we will demonstrate our recent findings on the mechanisms of telomerase activation in vascular smooth muscle cells (VSMCs)[5] and discuss the pathophysiology of telomere and telomerase activity in vascular diseases.

Telomerase activity in VSMCs

Association of telomerase activity with VSMC growth

We initially found that significant telomerase activity was present in proliferating VSMCs, which was decreased with cell confluency and was greatly suppressed upon serum deprivation. To investigate the association
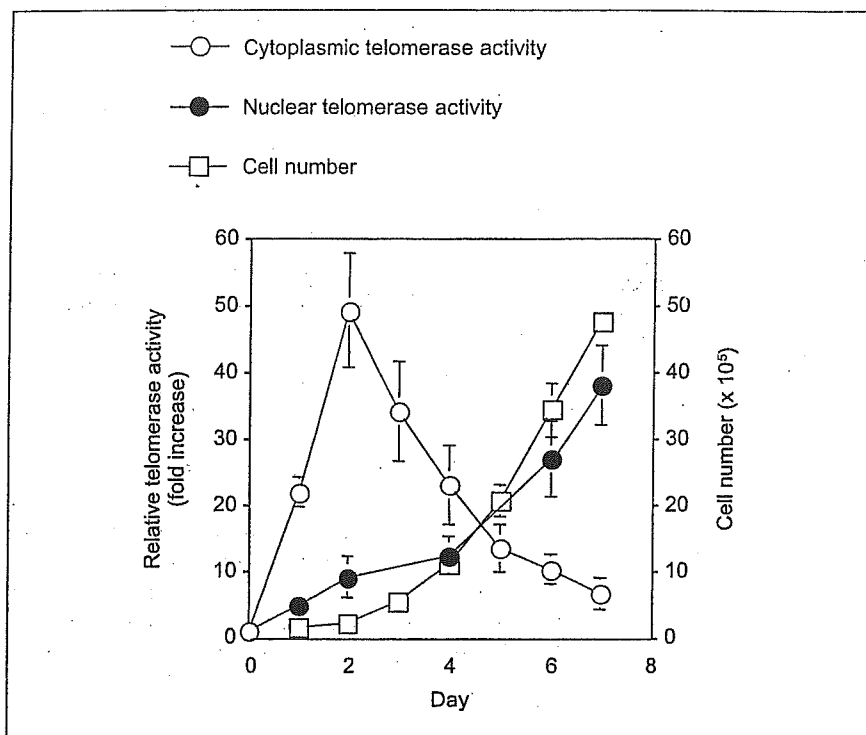
Fig. 1. The association of telomerase activity with cell proliferation in vascular smooth muscle cells. Time course of relative cytoplasmic and nuclear telomerase activity compared with cell number. The values plotted are relative to telomerase activity at day 0. The viable cell number was determined at each time point using trypan blue exclusion, and cell number per 100 mm-diameter plate is indicated (n = 6).

of telomerase activity with cell proliferation, we examined telomerase activity during proliferation in primary cultures of VSMCs after serum stimulation. Proliferating cells were harvested every 24 hours (days 1–7), and cytoplasmic and nuclear extracts were prepared and subjected to telomerase assay. Cytoplasmic telomerase activity was increased with a peak at day 2 (50-fold) but significantly decreased on days 3–7 at a time of active cell proliferation (Fig. 1). It is noteworthy that the induction of cytoplasmic telomerase activity appeared to precede cell proliferation, suggesting that telomerase activity may be involved in the modulation of cell proliferation in VSMCs. In contrast to cytoplasmic telomerase activity, nuclear telomerase activity was gradually increased with cell proliferation and reached levels 40-fold above baseline at day 7 (Fig. 1). Thus, most telomerase activity in the early phase of cell proliferation is localized in the cytoplasm, and during the log phase of cell growth it accumulates within the nucleus.

Telomerase inhibition reduces VSMC proliferation

To determine whether telomerase activation contributes to VSMC growth, we inhibited telomerase activity using a telomerase inhibitor TAG, hexameric, telomere-mimic phosphorothioate oligonucleotides (TTAGGG) that have been shown to suppress telomerase activity in cancer cells. VSMCs were stimulated to proliferate by addition of serum in the presence of TAG or scrambled phosphorothioate oligonucleotides, and cell number and telomerase activity were determined. As shown in Figure 2A, while scrambled oligonucleotides did not affect telomerase activity, TAG effectively inhibited the activity in a dose-dependent manner 2 days after treatment. Moreover, TAG significantly inhibited VSMC proliferation in a dose-dependent manner, as compared with control

cultures 4 days after treatment (Fig. 2B). Because a significant reduction in cell proliferation was observed within 4 days of telomerase inhibition, it is unlikely that progressive telomere shortening was responsible for decreased cell proliferation. Since we detected increased cyclin-dependent kinase (CDK) inhibitors in VSMCs treated with the telomerase inhibitor, reduced cell proliferation induced by telomerase inhibition may be attributed to induction of CDK inhibitors.

Mechanisms of telomerase activation in VSMCs

Expression of telomerase components

The mammalian telomerase RNA component (TERC) and two protein components, telomerase-associated protein 1 (TEP1) and telomerase reverse transcriptase (TERT), have been identified. Expression of TERC was shown to correlate with cell proliferation as well as telomerase activity in cancer cells. TERT mRNA levels were also reported to correlate with telomerase activity and to be implicated in the regulation of telomerase activity in cancer cells.[6] Furthermore, telomerase activity in telomerase-negative cells can be restored by ectopic expression of TERT,[7] suggesting that in certain cases, TERT is the only limiting factor for telomerase activation. TEP1 is known to be modified from p240 to p230, and the modification of TEP1 is implicated in the regulation of telomerase activity. To investigate potential regulatory mechanisms for telomerase activity, we examined levels of the various telomerase components during VSMC proliferation. Northern blot analysis showed that levels of the telomerase RNA component did not change with cell growth (Fig. 3A). Total protein levels of TEP1 did not change nor did the ratio of p230 to p240 protein levels (Fig. 3B). In contrast, TERT mRNA levels were induced with cell proliferation and reached fivefold above baseline at day 7. Western blot analysis for TERT demonstrated that expression of TERT was increased with cell proliferation
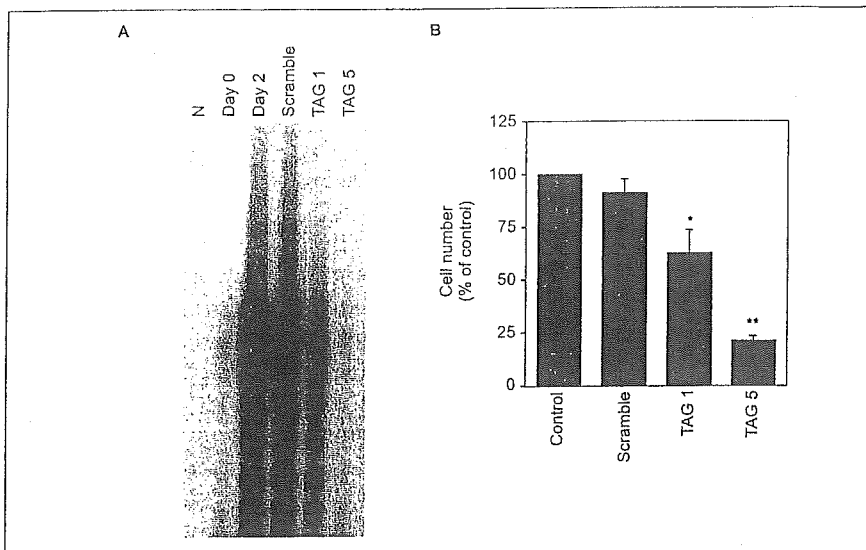
212

Fig. 2. Effects of telomerase inhibition on vascular smooth muscle cells (VSMC) proliferation. **A.** Inhibitory effects of TAG on telomerase activity. VSMCs deprived of serum for 7 days (day 0) were stimulated to proliferate by addition of 10% serum in the absence (day 2) or the presence of 1 μmol/L (TAG 1) or 5 μmol/L (TAG 5) of telomerase inhibitor, or scrambled phosphorothioate oligonucleotides (Scramble, 5 μmol/L). Two days after incubation, cytoplasmic extracts were analyzed for telomerase activity. Day 2 sample pretreated with RNase served as a negative control (N). **B.** Reduced cell growth induced by telomerase inhibition. VSMCs were stimulated to proliferate in the absence (Control) or the presence of telomerase inhibitor (TAG) or scrambled phosphorothioate oligonucleotides (Scramble). Four days after incubation, a cell number was determined using trypan blue exclusion. The values are relative cell number to the control at day 4. Data represent the mean ± S.E. (n = 4). TAG significantly inhibited VSMC proliferation in a dose-dependent manner (*$p < 0.0005$, **$p < 0.0001$ vs. Control, one way ANOVA).

Fig. 3. Expression of telomerase components in vascular smooth muscle cells. **A.** Northern blot analysis for telomerase RNA component. Ribosomal 28S was used for internal control (lower panel). **B.** Western blot analysis for TEP1 expression. The positions of p240 and p230 are indicated. **C.** Western blot analysis for TERT expression. Nuclear fractions and cytoplasmic fractions were assayed for TERT protein expression by Western blotting. Abbreviations: TERC, telomerase RNA component; TEP1, telomerase-associated protein 1; TERT, telomerase reverse transcriptase.

(Fig. 3C). Modestly increased levels of *TERT* mRNA and TERT protein levels appeared to be associated with increased telomerase activity. Taken together with the time course of telomerase activity in the cytoplasm and nucleus, these protein data indicate that accumulation of TERT in the nucleus may be at least partially responsible for the induction of nuclear telomerase activity.

Role of protein phosphorylation in the regulation of telomerase activity

We noted that telomerase activity was sensitive to the treatment with phosphatases. Since increased expression of the telomerase components in VSMCs could not account for the observed dramatic increase in cytoplasmic telomerase activity, we hypothesized that the activation of telomerase in the cytoplasm may be mediated by protein phosphorylation. To test our hypothesis, we examined the effects of kinase inhibitors on the activation of cytoplasmic telomerase in culture. Treatments with H7 and PKC inhibitory peptide and, to a lesser degree, PKA inhibitory peptide but not herbimycin A, tyrphostin, tyrosine kinase inhibitors or PD-98059, mitogen-activated protein kinase kinase inhibitors, reduced the activation of telomerase activity. These data suggest that telomerase is activated in the cytoplasm at least in part by protein phosphorylation, which is mediated by H7-sensitive kinase(s).

To determine whether protein phosphorylation promotes the accumulation of telomerase activity in the nucleus, we examined the effects of H7 on nuclear telomerase activity. Treatment of cells with H7 inhibited the accumulation of TERT as well as telomerase activity in the nucleus during VSMC proliferation in a dose-dependent manner but did not affect TEP1 levels in the nucleus (Fig. 4A). To confirm the effects of H7 on the accumulation of TERT in the nucleus, we established vascular smooth muscle cell lines that constitutively express TERT-FLAG protein and examined the
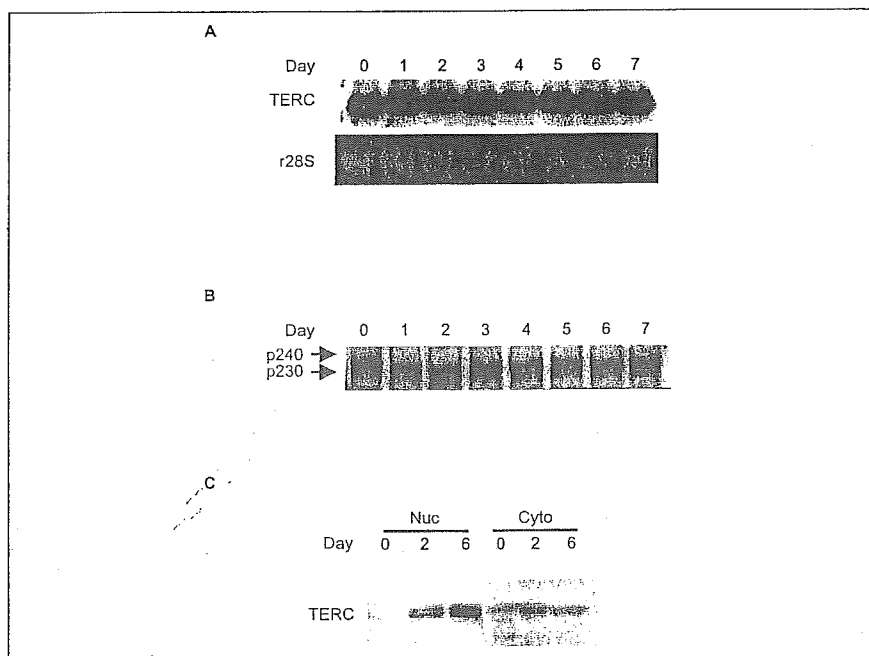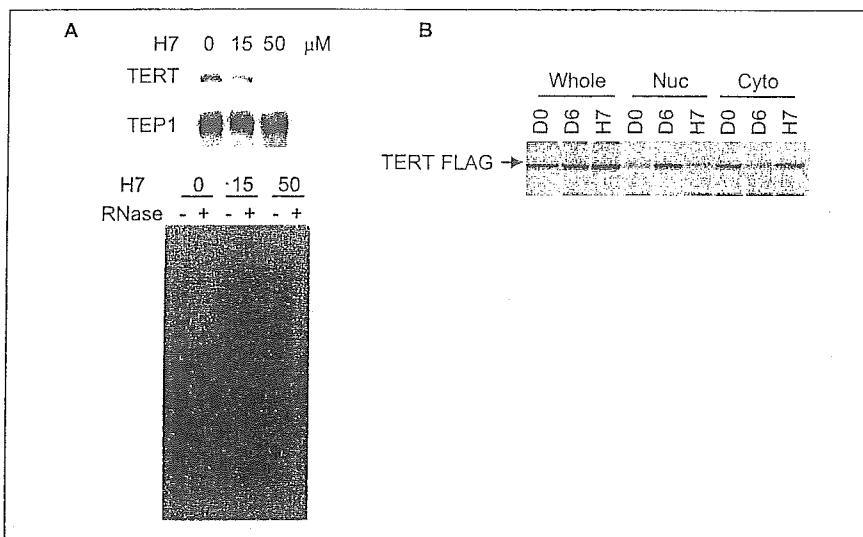
213

Fig. 4. Effects of protein kinase inhibitors on nuclear telomerase activity. **A.** Inhibitory effects of H7 on nuclear telomerase activity. Confluent cells deprived of serum for 7 days were subcultured in the presence of 10% serum with H7 at a concentration indicated. After 6 days, nuclear extracts were analyzed for TEP1 and TERT expression (upper panel) as well as telomerase activity (lower panel). **B.** Distribution of TERT-FLAG protein during cell growth. TERT-FLAG cells were deprived of serum for 3 days and subcultured in the presence of serum for 6 days with H7 (H7) or without H7 (D6). Whole-cell lysates (Whole), nuclear extracts (Nuc) and cytoplasmic extracts (Cyto) were prepared, and TERT-FLAG protein was then detected by Western blot analysis using anti-FLAG antibody.

Fig. 5. Phosphorylation of telomerase reverse transcriptase (TERT). **A.** Protein phosphorylation of TERT-FLAG *in vitro*. Cytoplasmic extracts from TERT-FLAG cells were subjected to *in vitro* kinase reaction in the presence of 1 mmol/1 ATP and 1 μCi/mcl [^{32}P] ATP for 0 minutes (lane 1) or 10 minutes (lane 2) with H7 (lane 3) or PKC inhibitory peptide (lane 4). *In vitro* kinase reaction mixtures were then immunoprecipitated with anti-FLAG antibody. One-tenth of each immunoprecipitate was also assayed for telomerase activity (lower panel). **B.** Protein phosphorylation of TERT-FLAG in vascular smooth muscle cells (VSMCs). VSMCs transfected with TERT-FLAG expression vector were labeled with ^{32}P-orthophosphate for 6 hours with (lane 2) or without H7 (lanes 1 and 3). TERT-FLAG protein was immunoprecipitated with anti-FLAG antibody in the absence (lanes 1 and 2) or the presence of FLAG peptide (lane 3). The immunoprecipitates were then subjected to SDS-PAGE analysis and transferred onto a PVDF membrane followed by autoradiography to detect phosphorylated TERT-FLAG (p-TERT FLAG) and immunoblotting with anti-FLAG antibody to detect immunoreactive TERT-FLAG (ir-TERT-FLAG).

distribution of TERT-FLAG during cell growth after serum stimulation. TERT-FLAG protein remained constant in whole cell extracts for the entire 6-day culture period, even in the presence of H7. However, TERT-FLAG was absent in nuclear extracts on day 0 and appeared on day 6, correlating with maximal nuclear telomerase activity. Conversely, it was detected in cytoplasmic extracts on day 0 but was absent on day 6. Treatment of cells with the kinase inhibitor H7 prevented the detection of TERT-FLAG in the nucleus (Fig. 4B). Inhibitory effects of H7 on TERT translocation into the nucleus were also demonstrated by metabolic labeling experiments. Taken together, these data indicate that protein phosphorylation is required for the accumulation of TERT as well as telomerase activity in the nucleus.

Since TEP1 protein levels in the nucleus were unaffected by treatment with H7, we speculated that protein phosphorylation of TERT might be responsible for activation and accumulation of telomerase in the nucleus in VSMCs. Cytoplasmic extracts from TERT-FLAG cells were subjected to *in vitro* kinase reaction in the presence of [^{32}P] ATP plus H7 or PKC inhibitory peptide followed by immunoprecipitation with anti-FLAG antibody (Fig. 5A). Although TERT-FLAG was phosphorylated in control extracts, the presence of H7 or PKC inhibitory peptide inhibited this phosphorylation and correlated with the presence or absence of telomerase activity in the respective extracts. Orthophosphate labeling experiments demonstrated that phosphorylated TERT-FLAG was detected in VSMCs, whereas preincubation with FLAG peptide completely abolished detection of phosphorylated TERT-FLAG as well as immunoreactive TERT-FLAG. Treatment with H7 inhibited phosphorylated TERT-FLAG detection, but immunoreactive TERT-FLAG was unaffected (Fig. 5B). Thus, protein phosphorylation of TERT may be an important mechanism underlying the regulation of telomerase activity in VSMCs. We hypothesize that TERT
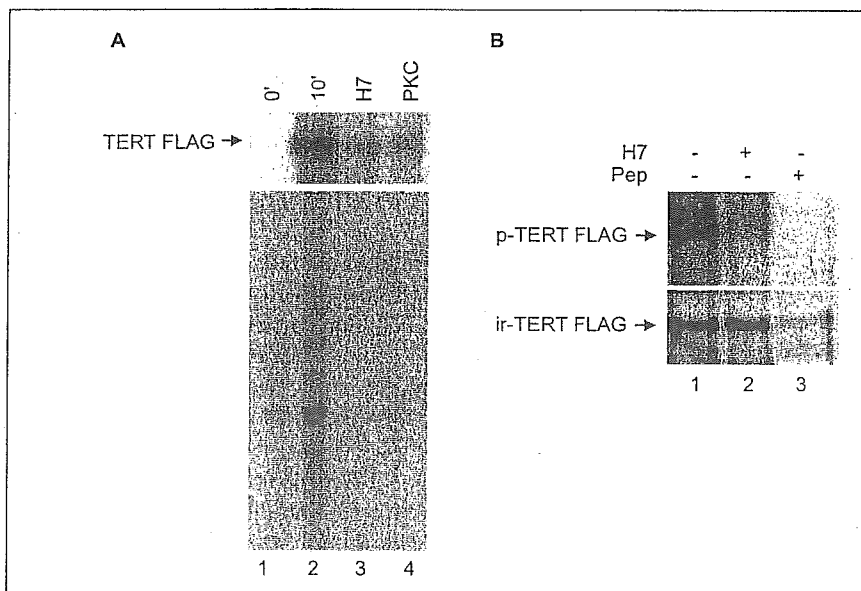
214

exists in the cytoplasm in an inactive, unphosphorylated state in unstimulated cells, but upon stimulation, protein phosphorylation permits nuclear localization of TERT, thereby allowing for assembly of active telomerase and function on telomeres.

Pathophysiology of telomere and telomerase activity

Restenosis after vascular injury

Cardiovascular interventions to correct arterial occlusive disease have excellent short-term results, but long-term patency is still seriously compromised by the development of restenosis. The pathophysiology of restenosis involves direct injury to VSMCs, leading to VSMC proliferation and migration into the intima. There is recent evidence that telomerase activation correlates with the occurrence of coronary artery restenosis. To explore the role of telomerase in regulating VSMC growth in injured artery, we examined telomerase activity in the rat vascular injury model. Two days after vascular injury, telomerase was markedly activated, which was significantly suppressed by the treatment with the telomerase inhibitor. Consequently, the neointimal formation was greatly reduced by inhibition of telomerase activity (Fig. 6). Thus, these findings establish a critical role for telomerase activation in the control of VSMC proliferation in injured artery.

Hypertension

The hallmark of chronic hypertension is vascular structural changes, including vessel wall hypertrophy and hyperplasia, which are major contributors to elevated resistance in hypertension. In spontaneously hypertensive rats (SHRs), a widely used model of human essential hypertension, vascular hypertrophy develops before any significant elevation in blood pressure, with increases in both the number and size of VSMCs. Using this genetic model for hypertension, Cao et al.[8] demonstrated a pivotal role of telomerase activity in the pathogenesis of hypertension. The increased telomerase activity was found in the aorta of
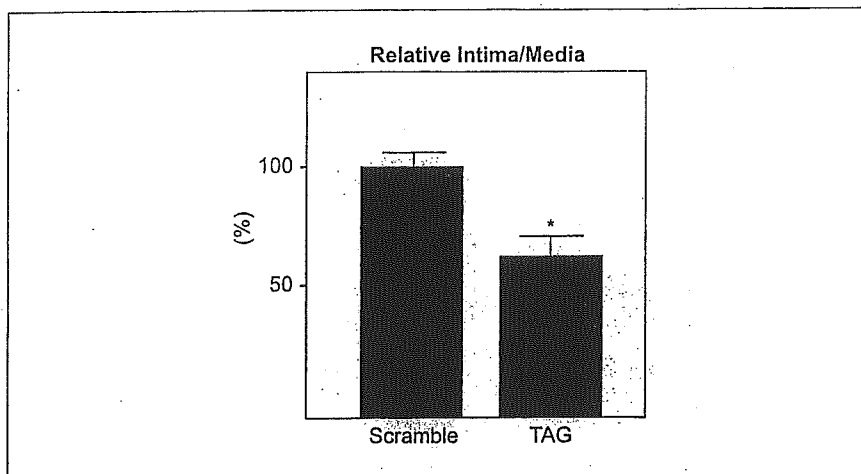

Fig. 6. Relative ratio of intimal area to medial area after injury. Fourteen days after vascular injury, the intima/media ratio was significantly decreased by inhibition of telomerase activity ($*p < 0.05$ vs. Scramble, unpaired t-test).

SHRs compared with normotensive control rats. This increase in the activity was detected as early as 3 weeks after birth, well before the onset of hypertension. Induction of TERT appeared to be attributed to telomerase activation in the aorta of SHRs. As a result of the activation, telomeres were lengthened in SHRs. It is noteworthy that there was no difference in telomere length and telomerase activity in other tissues between SHRs and the control rats. Thus, the selective activation of telomerase in the aortic tissues of SHRs is not secondary to high blood pressure but underlies vessel wall proliferation during the development of hypertension.

Vascular Aging

Age-associated changes in the blood vessels include a decrease in compliance and an increase in inflammatory response that promote atherogenesis.[9] The stiffness of aged arteries has been attributed to age-associated functional changes in VSMCs, including an increase in collagen synthesis and elastase activity, and impaired endothelial-independent relaxation. Endothelial-dependent vasodilatation also decreases with age because of a decrease in endothelial production of nitric oxide and prostacyclin as well as a decrease in sensitivity of VSMCs to these vasodilators. Moreover, in-

creased expression of proinflammatory and prothrombogenic molecules is observed in vascular cells of aged arteries. Of interest is that similar functional changes have been reported in senescent vascular cells in vitro.

Cellular senescence is the limited ability of primary human cells to divide when cultured in vitro and accompanied by a specific set of phenotypic changes in morphology, gene expression and function. These changes in phenotype have been implicated in human aging, including atherosclerosis.[10] Consistent with this notion, we have recently shown the presence of senescent vascular cells in human atherosclerosis.[11] We have also shown that introduction of telomere dysfunction results in an impairment of vascular function as seen in aged artery, whereas telomerase activation restored vascular dysfunction associated with senescence (Fig. 7). Moreover, progressive telomere shortening has been reported in human atherosclerotic lesions.[12] It is assumed that an increased rate of cell turnover in the lesions accelerates progressive telomere shortening and vascular cell senescence, which contributes to vascular dysfunction. Thus, activation of telomerase may be beneficial for the treatment of vascular aging.
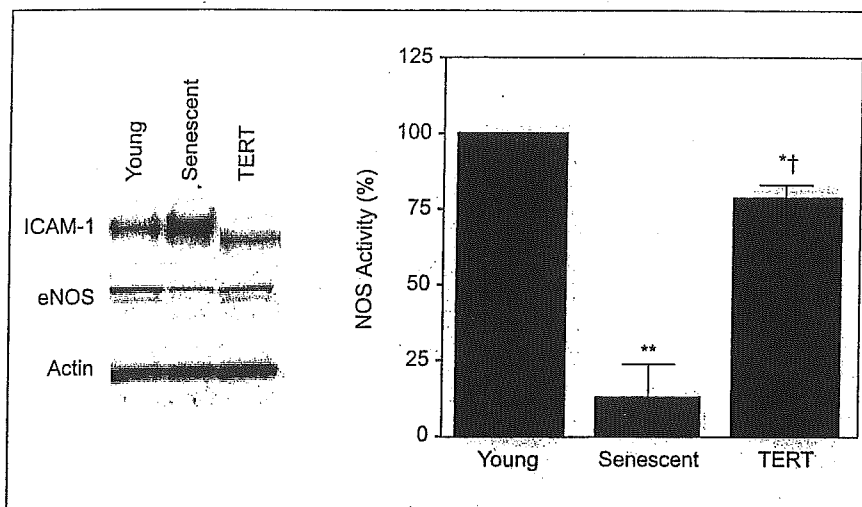
Fig. 7. Introduction of telomerase preserves vascular dysfunction associated with senescence. Western blot analysis of intercellular adhesion molecule (ICAM-1) and endothelial nitric oxide synthase (eNOS), and eNOS activity in parental young vascular cells, senescent cells and TERT-infected cells. The NOS activity in parental cells is set at 100% and compared with that in senescent cells and cells infected with TERT (right graph, n = 4, $*p < 0.05$ vs. parental, $**p < 0.001$ vs. parental, $\dagger p < 0.01$ vs. senescent, ANOVA).

Chronic hypoxia

Chronic hypoxia has been shown to promote proliferation of VSMCs, leading to vascular remodeling, a key pathologic component of pulmonary hypertension. We demonstrated that chronic hypoxia prolonged cell lifespan of VSMCs and was associated with telomere stabilization and telomerase activation.[13] Hypoxia significantly induced phosphorylation of TERT, resulting in increased telomerase activity. TERT protein levels remained elevated under hypoxia compared with those found under normoxia for significantly longer population doublings. Furthermore, inhibition of telomerase shortened cell lifespan of hypoxic cultures, whereas constitutive expression of TERT extended cell lifespan. These findings argue that telomerase activity can be modulated in the vasculature in response to hypoxia and regulate cell lifespan of VSMCs and, ultimately, vascular functions.

Hyperoxia and oxidative stress have been known to induce cellular senescence and contribute to organismal aging. Since under normoxic conditions, cells were exposed to 21% oxygen, a significantly higher level of oxygen than is normally present in the arterial wall *in vivo*, our data on the proliferative vascular effects of low oxygen suggest that oxidative stress accelerates telomere loss through telomerase inactivation, which may underlie the pathophysiology of cellular senescence associated with vascular aging.

Conclusion

Telomere biology in the vasculature has begun recently and is still in its infancy. However, recently accumulating evidence indicates that telomerase activity is involved in the pathogenesis of human vasculopathies. Inhibition of telomerase may be effective therapeutic strategy for proliferative vascular disorders such as restenosis after angioplasty, whereas introduction of telomerase may restore vascular dysfunction associated with human aging. Further studies on telomerase and telomere function would be crucial for developing novel treatments for vascular disease.

References

1. Greider, C.W. *Telomere length regulation*. Annu Rev Biochem 1996, 65: 337–65.

2. Holt, S.E. and Shay, J.W. *Role of telomerase in cellular proliferation and cancer.* J Cell Physiol 1999, 180: 10–8.

3. Greenberg, R.A., Chin, L., Femino, A. et al. *Short dysfunctional telomeres impair tumorigenesis in the INK4a(delta2/3) cancer-prone mouse.* Cell 1999, 97: 515–25.

4. Lee, H.W., Blasco, M.A., Gottlieb, G.J., Horner, J.W., II, Greider, C.W. and DePinho, R.A. *Essential role of mouse telomerase in highly proliferative organs.* Nature 1998, 392: 569–74.

5. Minamino, T. and Kourembanas, S. *Mechanisms of telomerase induction during vascular smooth muscle cell proliferation.* Circ Res 2001, 89: 237–43.

6. Liu, J.P. *Studies of the molecular mechanisms in the regulation of telomerase activity.* FASEB J 1999, 13: 2091–104.

7. Bodnar, A.G., Ouellette, M., Frolkis, M. et al. *Extension of life-span by introduction of telomerase into normal human cells.* Science 1998, 279: 349–52.

8. Cao, Y., Li, H., Mu, F.T., Ebisui, O., Funder, J.W. and Liu, J.P. *Telomerase activation causes vascular smooth muscle cell proliferation in genetic hypertension.* FASEB J 2002, 16: 96–8.

9. Cooper, L.T., Cooke, J.P. and Dzau, V.J. *The vasculopathy of aging.* J Gerontol 1994, 49: B191–6.

10. Faragher, R.G. and Kipling, D. *How might replicative senescence contribute to human ageing?* Bioessays 1998, 20: 985–91.

11. Minamino, T., Miyauchi, H., Yoshida, T., Ishida, Y., Yoshida, H. and Komuro, I. *Endothelial cell senescence in human atherosclerosis: Role of telomere in endothelial dysfunction.* Circulation 2002, 105: 1541–4.

12. Chang, E. and Harley, C.B. *Telomere length and replicative aging in human vascular tissues.* Proc Natl Acad Sci USA 1995, 92: 11190–4.

13. Minamino, T., Mitsialis, S.A. and Kourembanas, S. *Hypoxia extends the life span of vascular smooth muscle cells through telomerase activation.* Mol Cell Biol 2001, 21: 3336–42.

Tohru Minamino*, M.D., Ph.D., is Research Associate and Issei Komuro, M.D., Ph.D., is Professor in the Department of Cardiovascular Science and Medicine, Chiba University Graduate School of Medicine, 1-8-1 Inohana, Chuo-ku, Chiba 260-8670, Japan.

E-mail: t_minamino@yahoo.co.jp.

*Correspondence.

216

CASE REPORT

Nobusada Funabashi · Masayori Yonezawa
Yoshito Iesaka · Hideo Umekita · Noriyuki Yanagawa
Yasunori Matsumoto · Katsuya Yoshida · Issei Komuro

Complications of pulmonary vein isolation by catheter ablation evaluated by ECG-gated multislice computed tomography

Abstract As pulmonary vein (PV) isolation by catheter ablation for paroxysmal atrial fibrillation may cause PV luminal stenosis, digital subtraction angiography or magnetic resonance imaging have been used to evaluate the lumen of the PV. Electrocardiogram-gated multislice computed tomography can evaluate the lumen of the PV from any plane desired after acquisition with excellent spatial resolution. It can also evaluate hyperplasia of soft tissue around the lumen of the PV, which cannot be evaluated by digital subtraction angiography, and may thus serve as an indicator of complications or even the effectiveness of this treatment.

Key words Pulmonary vein isolation · Catheter ablation · ECG-gated multislice computed tomography · Luminal stenosis · Hyperplasia of soft tissue

Introduction

The catheter ablation procedure has been performed to treat arrhythmias such as lone atrial fibrillation (Af).[1-7] Application of this procedure to the ostium of the pulmonary vein (PV), called PV isolation, which adjusts paroxysmal lone Af without any organized heart disease, may cause luminal stenosis of the PV due to hyperplasia of the vessel wall or loss of vessel smooth muscles.[4,8-10] Therefore,

it is necessary to evaluate the PV after the procedure using diagnostic modalities such as digital subtraction angiography (DSA), magnetic resonance imaging (MRI), intracardiac echocardiography,[10] and transthoracic echocardiography. However, DSA and intracardiac echocardiography are invasive, transthoracic echocardiography is highly dependent upon the skill of the operators, and it is difficult to evaluate the degree of hyperplasia of the PV wall with DSA. The newest multislice computed tomography (MSCT) with electrocardiogram (ECG)-gated acquisition can acquire excellent images without cardiac motion artifacts and also obtain volumetric data that continues to the through-plane with excellent quality, allowing the evaluation of the vessel lumen in any plane desired by a three-dimensional reconstruction technique as well as in the axial source images.[11] Furthermore, MSCT can detect hyperplasia of soft tissue around the vessel lumen due to its excellent contrast resolution.

Case report

A 50-year-old woman underwent radiofrequency (RF) catheter ablation by the trans-septal technique for lone Af without any organic heart disease. A decapolar catheter, a quadripolar catheter, and a circular decapolar catheter (Lasso, Biosense Webster, Markham, ON, Canada) were inserted through the right femoral or subclavian veins and placed in the coronary sinus, left atrial appendage (LAA), and proximal lumen of the targeted PV close to the PV ostium. Selective PV angiography was performed by hand injection of 10 ml of contrast medium through a long sheath. No pre-existent stenosis was demonstrated.

RF ablation of PVs was targeted to the ostial portion of the breakthrough segments connecting the left atria (LA) to the PV, which were identified as the earliest PV potentials (PVPs) recorded from the circular catheter in the right superior, left superior, or left inferior PVs in sinus rhythm or during pacing from the LAA. The right inferior PV did not require ablation because no PV potentials were re-

N. Funabashi (✉) · M. Yonezawa · Y. Matsumoto · K. Yoshida · I. Komuro
Department of Cardiovascular Science and Medicine, Chiba University Graduate School of Medicine, 1-8-1 Inohana, Chuo-ku, Chiba 260-8670, Japan
Tel. +81-432-26-2097; Fax +81-432-26-2557
e-mail: nobusada@ma.kcom.ne.jp

Y. Iesaka
Cardiovascular Center, Tsuchiura Kyodo Hospital, Tsuchiura, Japan

H. Umekita · N. Yanagawa
Division of Radiology, Chiba University Hospital, Chiba, Japan